Journal of the Energy Institute 129 (2026) 102685

Contents lists available at ScienceDirect

Journal of the Energy Institute

journal homepage: www.elsevier.com/locate/joei

Dynamics, frequency and oscillation characteristics of near-blowout plasma stabilized flames in a swirled burner using high-speed chemiluminescence and spectral mode decomposition methods

Sara Bonuso [a], Ghazanfar Mehdi [b], Stefan Raphael Harth [c], Elisa Pescini [d], Ossi Kaario [b], Maria Grazia De Giorgi [a,*]

[a] Department of Engineering for Innovation, University of Salento, Lecce, 73100, Italy
[b] Department of Energy and Mechanical Engineering, Aalto University, School of Engineering, Espoo, 02150, Finland
[c] Combustion Technology, Engler-Bunte-Institute, Karlsruhe Institute of Technology, Karlsruhe, 76131, Germany
[d] Departamento de Tecnología y Ciencias Aeroespaciales, Centro Universitario de la Defensa, Universidad Politécnica de Cartagena member of European University of Technology EUT+, C/Coronel López Peña S/N, Base Aerea de San Javier, Santiago de La Ribera, Murcia, 30720, Spain

ARTICLE INFO

Keywords:
Plasma-assisted combustion
Sinusoidal discharge
Flame morphology
Spectral orthogonal decomposition
Chemiluminescence

ABSTRACT

This experimental study investigates the influence of sinusoidal plasma discharges on low-swirled methane/air flames, exploring conditions ranging from stable operation to near-lean blowout. A ring-needle plasma actuator operating at 20 kHz near the nozzle exit is used, and high-speed chemiluminescence diagnostics track the spatial and temporal flame dynamics. Plasma actuation significantly reduces the flame lift-off height by approximately 20 mm and decreases the variance in OH* chemiluminescence intensity by 30%, enhancing flame stability. Flame morphology changes are quantified using image processing techniques, including Zernike coefficients, Hu moments, curvature, perimeter, area, and centroid coordinates. These analyses provide a detailed description of flame shape variations under different operating conditions. Advanced decomposition techniques, such as Proper Orthogonal Decomposition (POD) and Spectral Proper Orthogonal Decomposition (SPOD), reveal dominant flame structures and frequency fluctuations. Phase Portrait POD and Autocorrelation SPOD Modes show a marked reduction in oscillatory amplitudes, highlighting the plasma's stabilizing effects. Plasma discharges redistribute energy from the dominant first mode to higher modes, reducing heat fluctuations and suppressing instabilities. This leads to a more uniform energy distribution across the flame, improving combustion efficiency. Acoustic measurements, analyzed through Fast Fourier Transform (FFT) and Wavelet Decomposition, correlate with imaging results, providing a comprehensive understanding of plasma's influence on both chemiluminescence and acoustic flame properties. These findings demonstrate that plasma effectively dampens high-frequency oscillations, redistributes energy, and enhances combustion stability, particularly near the lean blowout limit.

1. Introduction

Premixed lean combustion concepts represent one of the most effective strategies to achieve low flame temperatures and consequently reduce NOx emissions [1] [2]. However, operating under lean conditions makes flames highly susceptible to instabilities that may lead to re-ignition issues and flame blowout [3]. In turbulent jet flames, the lift-off phenomenon has attracted considerable attention for both commercial and military applications, although it may also generate undesirable effects such as increased noise, leakage of unburnt fuel, and flame extinction. The prediction and modelling of lift-off height in turbulent gaseous flames have been addressed by Sarras et al. [4], demonstrating the strong coupling between turbulence characteristics and flame stabilization mechanisms in natural gas configurations.

Lean blowout (LBO) commonly occurs in lifted flames, and its physical mechanisms are not yet fully understood. As a result, flame stabilization remains a critical challenge in aero-engines and gas turbine combustors [5], [6]. Several strategies have been proposed to enhance flame stability, including bluff bodies, swirl stabilization, pilot flames, and oxygen-enriched co-flow configurations [5]. Nevertheless, these

* Corresponding author.
E-mail address: mariagrazia.degiorgi@unisalento.it (M.G. De Giorgi).

https://doi.org/10.1016/j.joei.2026.102685
Received 27 May 2026; Received in revised form 28 July 2026; Accepted 5 August 2026
Available online 6 August 2026
1743-9671/© 2026 The Authors. Published by Elsevier Ltd on behalf of The Energy Institute. This is an open access article under the CC BY license (http://creativecommons.org/licenses/by/4.0/).

approaches often introduce permanent geometric modifications or additional system complexity, limiting their applicability in practical systems. Similar challenges related to LBO and lifted flame dynamics in turbulent combustors have recently been investigated by Morales et al. [7], who employed modal and high-speed diagnostic techniques to characterize turbulence-driven extinction mechanisms and coherent oscillatory structures preceding blowout.

Among the emerging active control strategies, plasma-assisted combustion (PAC) has gained significant attention for its capability to enhance ignition, extend flammability limits, and improve flame stabilization while reducing pollutant emissions [8] [9] [10]. Plasma effects on combustion can generally be classified into thermal, chemical, and aerodynamic contributions. In recent years, research has primarily focused on non-thermal plasma (NTP) technologies [11] [12] [13]. In NTP systems, energetic electrons collide with fuel molecules, generating highly reactive radicals and excited species that accelerate chemical reaction pathways. In addition, ionic wind produced by plasma discharges enhances fuel–air mixing and promotes chain oxidation reactions, thereby accelerating the overall combustion process [14] [15].

Plasma generation through electrical discharges can be achieved using several configurations, including dielectric barrier discharge, corona discharge, pulsed discharge, microwave discharge, glow discharge, and high-frequency discharge [16]. Among these technologies, corona discharge plasma has been widely investigated due to its relatively simple configuration, operational flexibility, and cost effectiveness [9] [16] [17] [18]. In such systems, plasma is typically generated between a high-voltage electrode with a sharp geometry and a grounded electrode [16] [19].

Several experimental studies have explored the role of plasma actuation in extending LBO limits and improving flame stabilization. For instance, Sun et al. [20] investigated the stabilization of premixed swirl flames using microsecond repetitively pulsed plasma discharges, demonstrating improved ignition delay times and extended blowout limits. Feng et al. [21] studied plasma-assisted ignition in a swirl combustor using a rotating gliding arc discharge, reporting enhanced ignition performance and improved stability. Varella et al. [22] analyzed the impact of PAC on pollutant emissions in premixed natural gas flames, observing a reduction in hydrocarbon and carbon monoxide emissions accompanied by increased oxidation efficiency. More recently, gliding-arc plasma actuators have also attracted considerable attention because of their capability to improve flame stabilization, extend lean blowout limits and enhance combustion under demanding operating conditions. Recent studies of Yifu Tian et al. [23] [24] demonstrated that gliding-arc plasma promotes ignition enhancement, suppresses flame blowout and improves flame robustness through combined thermal, chemical and aerodynamic effects.

Despite these promising results, the complex interactions between plasma discharges, flow dynamics, and combustion chemistry remain only partially understood. In particular, the effect of plasma actuation on lifted flame stabilization and LBO limits is still largely exploratory. Mehdi et al. [9] [25] [26] [27], Fontanarosa et al. [10], and De Giorgi et al. [28] [29] conducted both numerical and experimental investigations on swirled methane/air combustors using sinusoidal and nanosecond pulsed plasma actuators to study ignition delay times, flammability limits, and flame propagation speed. More specifically, De Giorgi et al. [28] and Bonuso et al. [30] investigated LBO limits in swirl-stabilized methane/air flames using a sinusoidally driven plasma reactor. Their experiments, supported by smoke flow visualization, demonstrated that plasma discharges significantly modify the flow field near the burner exit. The sensitivity of premixed swirling flames to vortex dynamics and flow-field modifications has also been highlighted by Ercole et al. [31], who showed how coherent turbulent structures strongly influence flame anchoring and stability.

However, only a limited number of quantitative experimental studies have investigated sinusoidally driven plasma-assisted lifted methane/air flames. Consequently, the dynamic response of lifted flames to sinusoidal plasma discharges remains insufficiently understood. Achieving effective combustion instability control requires a deeper understanding of the transient processes associated with plasma–flame interaction. This need for further investigation has also been highlighted in the review by Li et al. [15]. To address these challenges, advanced optical diagnostics are increasingly employed to characterize flame dynamics and structure in combustion systems [32].

Among non-intrusive diagnostic techniques, high-speed imaging combined with advanced data analysis methods provides valuable insight into flame instabilities. Ruan et al. [33] described several optical diagnostics commonly used in gas turbine combustion research. In particular, Proper Orthogonal Decomposition (POD) has become a widely used tool for identifying coherent structures in turbulent reacting flows. POD provides an optimal representation of a flow field based on its energetic content, enabling the extraction of dominant spatial structures from fluctuating datasets [34] [35]. In reacting swirling flows, POD-based analyses have been successfully used to investigate the coupling between vortex structures and flame response under lean operating conditions [7].

The POD methodology was originally introduced in fluid mechanics by Lumley [36], while the snapshot approach for large datasets was later developed by Sirovich [37]. Mehdi et al. [26] [27] applied POD to analyse flow structures generated by nanopulsed plasma discharges in a swirled burner, demonstrating that plasma actuation significantly modifies the flow field near the burner exit. Similarly, POD analysis of OH* chemiluminescence images has been used to characterize flame instabilities in gas turbine combustors operating with Jet-A1 fuel [38]. Duwig et al. [39] further employed POD in extremely lean gas turbine combustion to investigate the interaction between swirl-induced vortex breakdown and large coherent flow structures.

In addition to POD, Spectral Proper Orthogonal Decomposition (SPOD) has recently emerged as a powerful technique for extracting coherent flow structures associated with specific frequency ranges [40] [41]. Unlike classical POD, SPOD identifies modes that are both spatially and temporally coherent by analysing the cross-spectral density of the dataset. This allows the decomposition of flow dynamics into frequency-resolved structures, providing deeper insight into oscillatory phenomena and instability mechanisms. SPOD has been applied in several areas of fluid mechanics and flow analysis, often in combination with other modal decomposition techniques such as Dynamic Mode Decomposition (DMD) and Koopman-based methods [42] [43].

The combined use of POD and SPOD techniques offers significant advantages in combustion diagnostics. While POD efficiently identifies the dominant energetic structures governing flame dynamics, SPOD enables the characterization of frequency-dependent phenomena, including resonant modes and periodic oscillations. Despite these advantages, SPOD has rarely been applied in combustion research and, to the best of the authors' knowledge, has not yet been employed to investigate plasma-assisted combustion systems.

The aim of this study is therefore to investigate the behaviour of attached and lifted methane/air flames in a plasma-assisted swirl combustor using a sinusoidal high-voltage excitation waveform. The study focuses on characterizing combustion dynamics through combined electrical, optical, and acoustic diagnostics. In particular, high-speed OH* chemiluminescence imaging is used to analyse the spatial and temporal evolution of the flame front, while the influence of plasma actuation on flame stability and lift-off height is evaluated across different equivalence ratios. Advanced modal decomposition techniques such as POD and SPOD are applied to characterize coherent structures and oscillatory dynamics. Additional analyses including flame morphology descriptors, Fast Fourier Transform (FFT), wavelet decomposition, and autocorrelation functions are used to investigate temporal fluctuations and combustion instabilities. Pressure oscillations are also measured using a calibrated microphone probe and analyzed through power spectral density and wavelet methods [44]. These combined diagnostic approaches provide a comprehensive understanding of plasma–flame interaction mechanisms and contribute to the development of advanced strategies for combustion stability control.

Novelty: The novelty of this work lies in several key aspects that distinguish it from previous studies in plasma-assisted combustion research:

1. **Innovative Burner Design**: A newly designed burner configuration is employed, as introduced in Ref. [28], enabling a unique investigation of plasma-assisted combustion dynamics.
2. **Sinusoidal Plasma excitation**: Unlike most studies based on nanopulsed generators, this work investigates plasma actuation using a sinusoidal generator, providing an alternative approach to plasma-assisted combustion.
3. **Application of SPOD in a near-blowout plasma stabilized flames:** One of the first applications of SPOD technique to sinusoidally plasma-actuated, lean, lifted swirl flames approaching lean blowout. In this specific configuration, SPOD provides a frequency-resolved characterization of the coherent flame structures and complements the conventional POD analysis.
4. **Advanced temporal analysis**: Phase portrait analysis, autocorrelation functions, and dynamic temporal analysis are integrated within the modal decomposition framework to investigate the evolution of plasma-induced instabilities.
5. **Quantitative Flame Morphology analysis**: Advanced image-processing techniques, including Zernike coefficients, Hu moments, curvature, perimeter, area, and centroid tracking, are used to quantitatively characterize the influence of plasma actuation on flame morphology.

2. Experimental characterization

2.1. Plasma combustion facility

In this study, a single burner with a square section area with a side length of 105 mm and 360 mm high was used to investigate the swirl lifted methane/air flames. The burner was surrounded by quartz glass from all sides to enable optical access for measurements and the top was left open to the ambient. Air was supplied to the system using a compressor while methane was provided by an external tank. The mass flow rate of air and fuel were measured using a mass flow meter with a precision of 2%. To generate swirl flames inside the burner, an atmospheric nozzle with a 319 mm^2 effective area was used, consisting of two co-rotating swirlers to provide rotary movement to the air before entering the burner. The primary swirler had a geometric swirl number of 0.76 and eight tangentially inclined vanes, while the secondary swirler had a swirl number of 0 and twelve straight vanes. The two vortices were separated by a prefilter, where primary and secondary air flows met at the prefilter blade and mixed with the fuel. The gaseous fuel was fed to the nozzle through eight holes in the primary swirler. Corona discharge plasma actuation was generated by the following arrangement: the nozzle acted as GND electrode and a needle (diameter of 1 mm and a length of 46 mm), placed at the center of the nozzle at a blunt tip angle of 90°, acted as HV electrode. To avoid interference of electromagnetic fields produced by plasma discharge, the test system was enclosed in a Faraday cage. Fig. 1 shows the sketch of experimental setup of plasma actuated lifted swirl combustor with the instrumentations and the real image of flame showing the axis of nozzle. More details on the experimental apparatus can be found in De Giorgi et al. [28].

2.2. Electrical characterization

The electrical setup included a HV sinusoidal amplifier (PVM500 Plasma Resonant and Dielectric Barrier Corona Driver), a current transformer (Bergoz CT-D1.0-B, ±0.5% accuracy), a HV probe (Tektronix P6015A, ±3% accuracy), an oscilloscope (R&S RTM3004), and a personal computer, as shown in Fig. 1. The generator supplied a sinusoidal voltage at constant frequency (~20 kHz) with variable amplitude. The HV probe was installed on the high-voltage side, while the current transformer was positioned on the grounded side. Both signals were simultaneously recorded via the oscilloscope.

Measurement accuracy was evaluated according to:

$$\textit{Measurement accuracy} = \pm \textit{ DC gain accuracy} \times |\textit{Reading net} - \textit{offset}| + \textit{Offset accuracy} \quad (1)$$

Signals were acquired at 25 MHz, capturing two periods (T) per

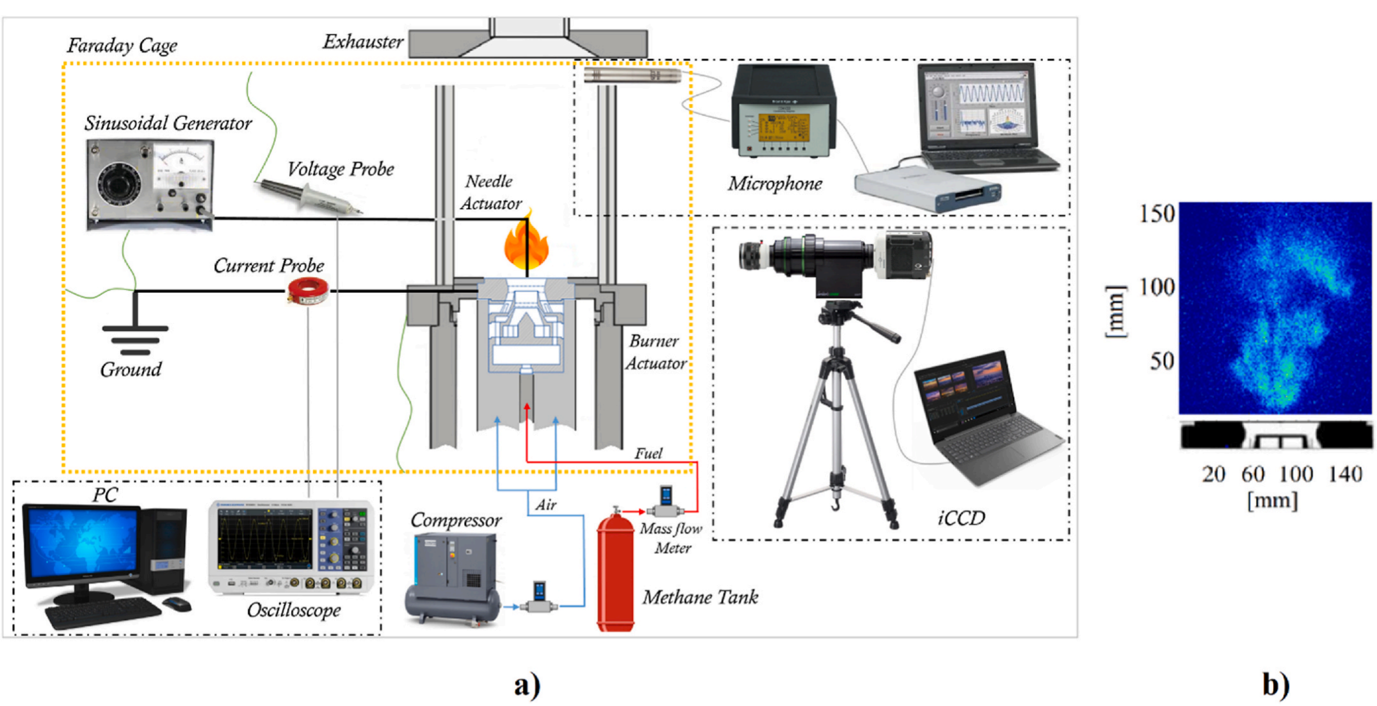

Fig. 1. a) Experimental instrumentation and setup of corona discharge plasma actuation in a lifted swirl combustor and b) real flame image.

acquisition. To enhance accuracy, 128 acquisitions were averaged. For each test case, voltage $V(t)$ and current $I(t)$ were recorded twice and averaged to obtain representative waveforms. The instantaneous electrical power $P'_{el}(t)$ was calculated by multiplying these two signals, and the mean electrical power dissipation P_{el} was evaluated over two periods:

$$P_{el} = {}^{1}/_{2T}\int_{0}^{2T} I(t)V(t)dt \tag{2}$$

Numerical integration was performed using the trapezoidal rule. The uncertainty of the calculated electrical power, estimated through standard uncertainty analysis methodology [45] [46], was approximately ±10%.

2.3. High-speed chemiluminescence flame imaging

High-speed OH* chemiluminescence was employed to characterize the plasma-assisted flame and investigate the spatio-temporal evolution of the flame front and primary reaction zone. In methane/air flames, OH* emission enables visualization of the instantaneous flame structure due to the high radical concentration at the reaction front. Images were acquired with identical ICCD settings for plasma and non-plasma cases at the same equivalence ratios to ensure direct comparison. Mean and variance fields were evaluated to quantify the effect of plasma actuation on flame stability.

Although line-of-sight OH* images do not exactly represent the true flame surface, they reliably capture global flame morphology and fluctuations. To quantify plasma-induced modifications, geometric and shape descriptors were extracted. Zernike coefficients were used to characterize asymmetry and higher-order shape variations, while Hu moments provided rotation- and scale-invariant features. Curvature, perimeter, and area were computed to assess flame front dynamics and size variations. Centroid coordinates (X, Y) were tracked to identify plasma-induced positional shifts. These metrics enable quantitative evaluation of morphological changes and stabilization mechanisms.

False-color maps of pixel luminance were used to visualize relative OH* intensity maxima, providing a qualitative indication of local heat release rate (HRR). Since HRR fluctuations are strongly linked to flame turbulence interactions and instability phenomena, temporal chemiluminescence variations were analyzed as indicators of flame stability.

OH* emissions were recorded using a Phantom M320S ICCD camera with Lambert image intensifier and narrow bandpass filters (Fig. 1). A UV lens (78 mm) and a 307 nm interference filter were used for OH* detection. Images were acquired at 1000 Hz with 8-bit resolution (0–255). MATLAB® user-defined routines were used for region of interest (ROI) selection, grayscale-to-luminance conversion (0–1), and dataset processing. The selected acquisition frequency of 1000 Hz represented a compromise between temporal resolution and sufficient OH* photon collection, image quality, and spatial resolution. The objective of the chemiluminescence measurements was not to resolve the individual plasma-discharge cycles occurring at approximately 20 kHz, but rather to characterize the lower-frequency flame response associated with lift-off dynamics, coherent flame oscillations, large-scale structures, and near-blowout behavior. Consequently, the corresponding Nyquist frequency is 500 Hz, and only flame dynamics below this limit can be reliably resolved. The reported spectral analyses therefore describe the low- and intermediate-frequency response of the flame to plasma actuation, whereas the 20 kHz excitation itself and any flame phenomena above 500 Hz are beyond the temporal resolution of the imaging system.

2.4. POD and SPOD analyses

POD and SPOD are the two data-driven techniques used for modal analysis of fluid flows. Extensive literature review about these methods is reported in Section 1.

POD technique was utilized to perform modal spatio-temporal characterization of the flame using high-speed acquisitions. POD is a dimensionality reduction technique that decomposes the flow of dynamic data into a set of orthogonal modes, ordered by their respective energy content, with the lowest order mode having the most energy. The energy contribution of each mode to the flow field reconstruction is described by their relative energy.

In brief, POD separates the spatial and temporal contributions of the generic flow data field by extracting an orthogonal basis of eigenvalues, such as:

$$g(x;\ t) = \Sigma_i\, g_i(x;t) = \Sigma_i\, a_i(t)\ \varphi_i(x) \tag{3}$$

where $a_i(t)$ represents the ith temporal eigenfunction, $\varphi_i(x)$ represents the ith spatial eigenfunction and x denotes the generic vector of spatial coordinates. Specifically, $a_i(t)$ brings information regarding the dynamics of the modal coherent structures, while $\varphi_i(x)$ involves obtaining a visual representation of the flow that captures the scales and shapes of the modal coherent structures. The energy contribution Λ, relative to the ith POD mode, in the image reconstruction is defined as:

$$\Lambda_i = \frac{\lambda_i}{\Sigma_{j=1}^{N_{POD}}\ \lambda_j} \tag{4}$$

where λ_i is the ith eigenvalue of the autocorrelation tensor. Two approaches exist: the snapshot method [47] and the direct method [48]. The first one was adopted due to the high spatial resolution and limited time history, yielding NPOD = N_{img}, where N_{img} is the number of images of the dataset.

SPOD extends POD to the frequency domain using Fourier-transformed flow data, enabling extraction of frequency-resolved coherent structures and associated energy content [48]. It identifies modes as eigenvectors of the Cross-Spectral Density (CSD) matrix at each frequency [40] [49].

The data matrix was segmented using the Welch method, assuming statistical independence between segments. A Discrete Fourier Transform (DFT) with Hamming windowing was applied to reduce spectral leakage [50]. For each frequency k, the weighted CSD matrix was computed as:

$$S_k = \frac{1}{N_b} W^{\frac{1}{2}} P_k^* P_k W^{*\frac{1}{2}} \tag{5}$$

where W defines the physical weighting and N_b is the number of Welch blocks [50]. Eigenvalue decomposition yields:

$$\mathrm{S_k} = \Psi_\mathrm{k}\ \Lambda_\mathrm{k}\ \Psi_k^* \tag{6}$$

where Λ_k represents the modal energy at frequency k [51].

POD provides global energetic structures, while SPOD resolves frequency-specific coherent dynamics. Their combined use enables cross-validation and comprehensive spatial–spectral characterization of plasma-assisted flame dynamics.

2.5. Microphone measurements

To capture the dynamics of the flame, acoustic measurements were conducted using a high sensitivity microphone (Bruel & Kjaer 4189 A 021), as shown in Fig. 1. The microphone was positioned outside the box, at a height of 39 cm from the burner outlet and at a radial distance of 11 cm from the burner center. Data were acquired using LabVIEW 2018 (NI) for 30 s at 10 kHz sampling frequency, enabling characterization of combustion-induced pressure fluctuations.

2.6. Wavelet decomposition and feature extraction

Wavelet decomposition provides time–frequency analysis of non-stationary signals through multiresolution representation. Unlike

Fourier analysis, wavelets employ adaptive temporal windows, offering high temporal resolution at high frequencies and high frequency resolution at low frequencies.

Signals are decomposed into approximation ("a", low-frequency) and detail ("d", high-frequency) components. The highest-frequency band corresponds to d_1, with subsequent bands (d_2, d_3, etc) halving in bandwidth successively. Pressure signals were decomposed using an eight-level discrete wavelet transform with a Daubechies-2 mother wavelet [44].

The wavelet energy at each scale is described using a specific formula:

$$p_j = E_j \Big/ \sum_{j=1}^{9} E_j \tag{7}$$

where E_j is defined as the sum of square of detailed wavelet transform coefficients, d_j:

$$E_j = \sum_k |d_j(k)|^2 \tag{8}$$

The wavelet entropy is another interesting variable that could be investigated [52]. In the present study, Shannon entropy [53] is used as measurement method. The Shannon entropy S provides a mathematical representation of the amount of uncertainty or information content within a given sequence and is expressed as follows:

$$S = -\sum_{j=1}^{9} p_j \, ln \, p_j \tag{9}$$

2.7. Experimental conditions

Experiments were performed with the plasma actuator both activated and deactivated. All the tests were performed under ambient conditions with a humidity of approximately 60%, a temperature of 298 K and an absolute pressure of 1 bar. Regarding the plasma excitation conditions, the power of the sinusoidal HV generator was set by fixing the voltage amplitude to 40% of the scale value and the frequency to maximum value (100% of the scale value). These settings were chosen to ensure a comparison between the conditions with and without plasma discharge at the same equivalence ratio Φ. During the tests, electrical characterization, chemiluminescence analysis, and flame dynamics characterization were performed. All these analyses were carried out with a fixed fuel flow rate of 1 m^3/h and the air mass flow rate was gradually decreased in order to obtain decreasing values of Φ (Φ = 1, 0.8, 0.58 and 0.45), thus gradually leaner flames, until the flame itself was extinguished. It is important to note that in the specific condition of Φ = 0.45 flame existence is observed solely in the presence of plasma actuation. LBO of the flame already occurs at Φ = 0.58. Table 1 provides the values of the peak-to-peak voltage, excitation frequency and mean electrical power P_{el} of the various tested conditions. Although variations in the flame environment may affect the electrical impedance of the plasma actuator, preliminary measurements performed at different equivalence ratios showed that the resulting variation in mean dissipated power was limited to approximately ±10%, which is lower than the estimated uncertainty of the measurement (±11%). Therefore, a single representative value of the mean electrical power is reported for the investigated plasma operating condition.

Table 1
Experimental conditions without and with sinusoidal HV generator.

Test case No.	Φ	HV generator	Voltage Peak-to-peak [V]	Repetition frequency [Hz]	Mean Electrical Power [W]
			[%V_{max}]	[%F_{max}]	
1.	1 0.8 0.58	None	-	-	-
2.	1 0.8 0.58 0.45	Sinusoidal	13572.8 40%	18994.3 100%	74 ± 8

3. Results and discussions

3.1. Electrical characterization

In this section, the electrical output results for the test cases in the presence of actuation are discussed. Table 1 shows the peak-to-peak voltage, repetition frequency, and mean electrical power delivered to the flame. It has to be noticed that the mean electrical power was equal to 74 ± 8 W.

Fig. 2 shows the temporal evolution of the voltage and current characteristics of the plasma actuator, along with the instantaneous electrical power generated during its operation. Fig. 2a shows the current waveform, which exhibits several high-amplitude spikes during the actuator operation, and the voltage waveform. Plasma discharges are known to be highly nonlinear phenomena and can introduce significant disturbances to the electrical circuit. The high-amplitude spikes observed in the current signals are indicative of these plasma discharges and can have a significant impact on the performance of the actuator. The discharge current exhibits a clear duality, with distinct positive- and negative-going cycles, reflecting the presence of two different micro-discharge phenomena. Notably, during the positive-going cycle, it can be observed occasional high current spikes, with the maximum current reaching approximately 100 mA. These spikes are associated with streamer discharges, which are filamentary in nature and release energy rapidly but briefly. Conversely, during the negative-going cycle, the glow-like discharges manifest as several lower-amplitude current pulses. It should be noted that these plasma micro discharges induce changes in the electrical impedance within the actuator, resulting in the occurrence of these current spikes. These spikes are characterized by an ultrashort duration and random timing, occurring within time intervals much shorter than the sinusoidal cycle period [54]. Therefore, it is crucial to monitor and analyse the electrical signals in order to gain a better understanding of the plasma actuator behavior and to optimize its performance. In addition to the voltage V(t) and current I(t) waveforms, Fig. 2b shows the instantaneous electrical power P'_{el} generated during the actuator operation. The electrical power waveform provides valuable information about the energy transfer within the actuator. Since the power is directly related to the voltage and current (see Equation (2)), the high amplitude spikes are also visible in the instantaneous electrical power waveform.

3.2. Spatial analysis of flame structures

3.2.1. Instantaneous, mean and variance of flame

This section analyzes the time-averaged and variance fields of OH* chemiluminescence to characterize flame stabilization under plasma and non-plasma conditions.

The investigated low-swirl flame is characterized by a lift-off behavior, with stabilization occurring downstream of the nozzle exit. The region preceding the primary reaction zone holds significant importance, as it facilitates the mixing of fuel and oxidizer without ignition, leading to flame reattachment, as demonstrated in recent literature of the present work authors [28] [55]. This stabilization mechanism relies on the upstream transport of hot vitiated gas from the main reaction zones through the Outer Recirculation Zone (ORZ) towards the initial region of the swirling jet [56].

Fig. 3 shows the comparative analysis of time-averaged and variance images of OH* chemiluminescence emissions considering the same equivalence ratios with or without the plasma actuation for various equivalence ratios (Φ = 1, 0.8, 0.58, and 0.45). It must be noticed that,

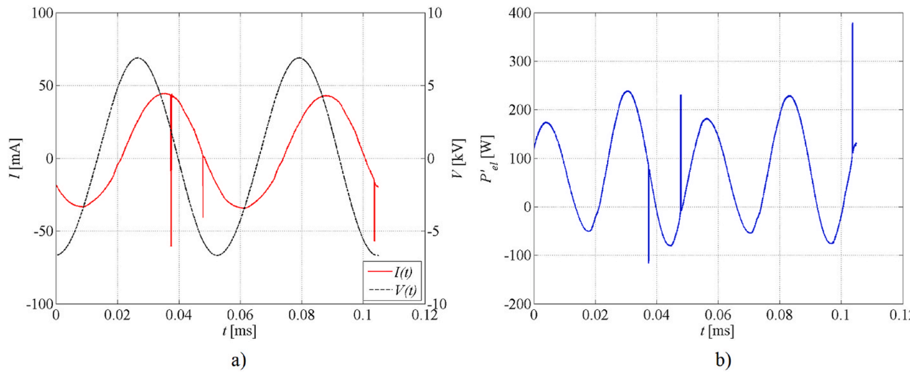

Fig. 2. *V(t)- I(t)* curves (left) and instantaneous electrical power temporal signal (right) for sinusoidal discharge.

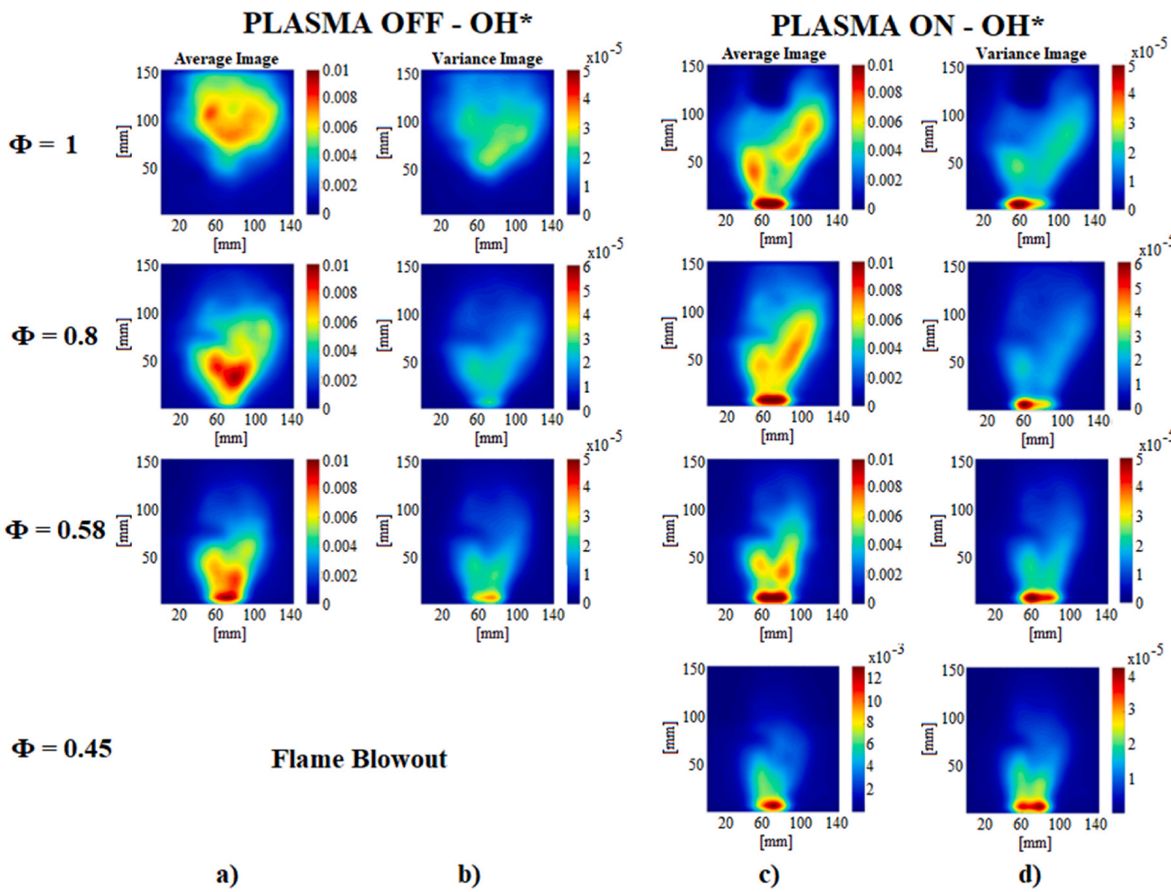

Fig. 3. Time-averaged (a – c) and variance (b – d) of the OH* chemiluminescence signal (line-of-sight) using same Φ (Φ = 1, 0.8, 0.58, and 0.45) for both Plasma OFF (a-b) and Plasma ON (c-d) conditions.

even if OH* emission images lack quantitative precision, images for both cases, with and without plasma discharge, are captured using identical camera settings. This ensures that relative differences between the two emission profiles can be effectively compared. It is noteworthy that the magnitudes of OH* emissions remain consistent between the cases with and without plasma actuation. At stoichiometric conditions ($\Phi = 1$), the baseline case without plasma actuation reveals a lifted flame with a lift-off height (LOH) of approximately 40 mm. The OH* emission zone appears less concentrated and more shifted downstream, suggesting a relatively unstable flame structure. As the equivalence ratio decreases ($\Phi = 0.8$ and 0.58), the OH* emission region gradually shifts closer to the nozzle exit, indicating a progressive reduction in LOH.

When plasma is applied, the OH* chemiluminescence becomes more intense and concentrates near the burner exit across all equivalence ratios. In particular, the presence of plasma generates a compact flame structure, clearly anchored closer to the nozzle. This is attributed to the generation of active radical species [25] [57] and enhanced mixing [55] induced by the high-frequency discharges, which increase the local concentration of reactive species and promote earlier heat release. Notably, at $\Phi = 0.45$, flame blowout occurs in the absence of plasma actuation due to strong instability and insufficient fuel reactivity. However, with plasma actuation, the flame is successfully sustained even at this low equivalence ratio.

The variance images confirm the stabilizing effect of plasma actuation. Without plasma, the OH* signal exhibits larger variance, indicating stronger fluctuations and instabilities in the flame front. In contrast, with plasma discharges, the variance is significantly reduced, implying a more stable and consistent flame structure. It is important to note that the elevated variance near the nozzle in plasma-assisted cases is partially attributed to the high-frequency nature of the discharges themselves, rather than flame instability. Since a plasma-only acquisition under non-reacting conditions was not performed, a contribution of direct plasma emission to the near-electrode OH* intensity fluctuations cannot be quantitatively excluded. Therefore, the variance increase in this region is interpreted cautiously and is not used as standalone evidence of modified flame dynamics. Moreover, the increased OH* concentration near the burner exit, combined with reduced fluctuations in the downstream flame zone, highlights the effectiveness of plasma actuation in anchoring and stabilizing the flame, even under lean and near-blowout conditions.

3.2.2. Geometric and morphological characterization of the flame

To quantitatively assess the impact of plasma actuation on the flame structure, geometric descriptors were extracted from the high-speed chemiluminescence images. The radar plots in Fig. 4 illustrate the variation of Zernike coefficients, Hu moments, mean curvature, area, perimeter, and centroid positions (X, Y) for OH* emissions under different Φ values, with (on the right) and without plasma (on the left).

For OH* emissions, a progressive variation in the shape descriptors is observed as the equivalence ratio decreases. At $\Phi = 1$, the descriptors

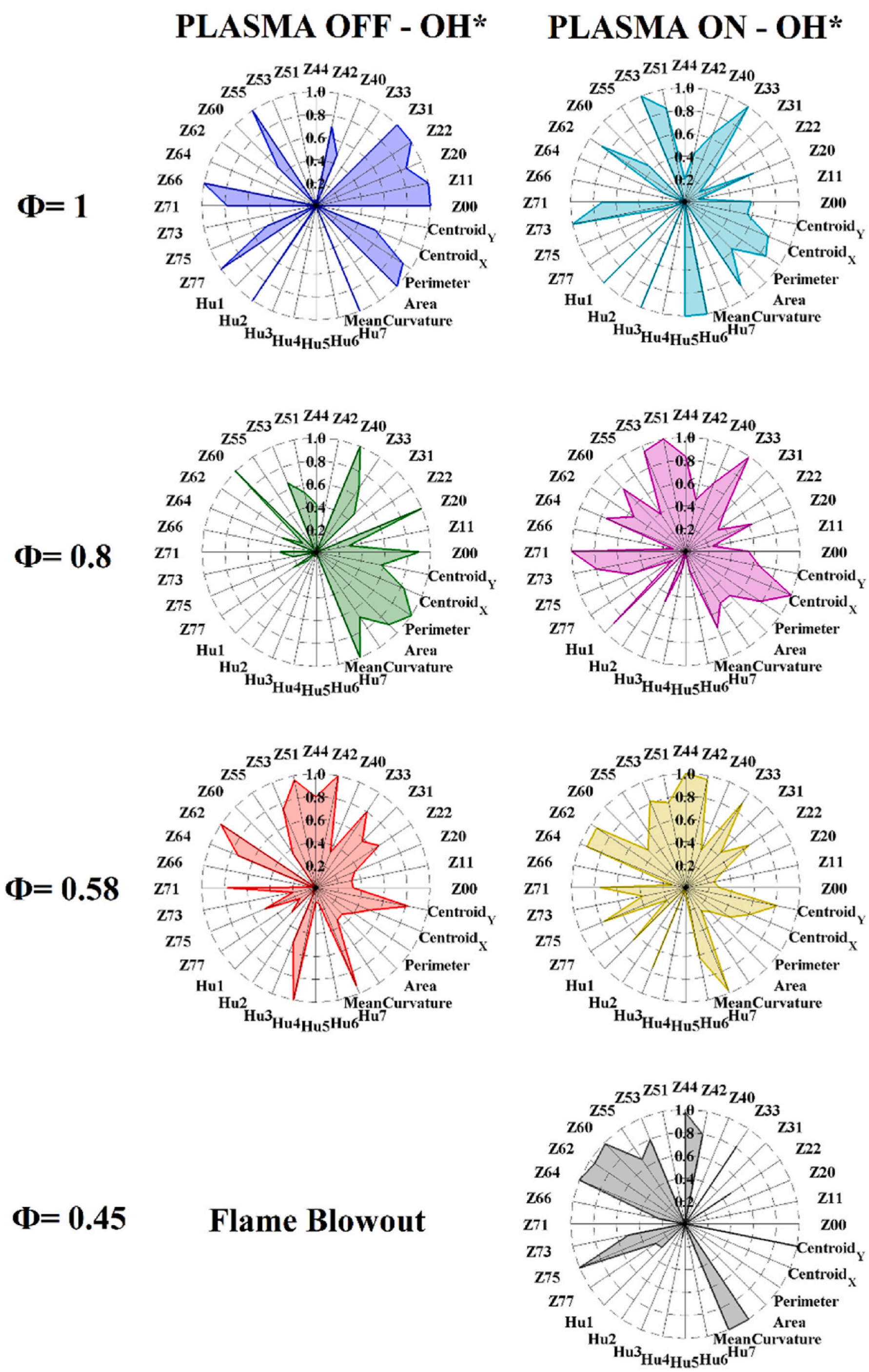

Fig. 4. Geometric descriptors of OH* for different Φ ($\Phi = 1$, 0.8, 0.58, and 0.45) with Plasma OFF and Plasma ON conditions.

exhibit higher symmetry, indicating a more structured flame. As Φ decreases, the variations in the Zernike coefficients and Hu moments become more pronounced, suggesting increased flame deformation and unsteadiness. In Fig. 4, the radar plots highlight that, at $\Phi = 0.8$ and $\Phi = 0.58$, the spread of the coefficients is significantly larger compared to $\Phi = 1$, indicating that the flame structure becomes more irregular and asymmetric. Notably, the lowest equivalence ratio ($\Phi = 0.45$ for the plasma case) exhibits a significant alteration in flame morphology, which is particularly evident in the OH* chemiluminescence results (on the right of Fig. 3). Here, the flame front shows a strong displacement, as seen in the centroid shifts, suggesting a substantial effect of plasma actuation on the reaction zone location.

The application of plasma significantly modifies the spatial characteristics of the flame. The radar plots indicate that plasma-actuated flames exhibit:

- A reduction in high-order Zernike coefficients, suggesting a smoother and more axisymmetric flame front at $\Phi = 1$. However, at lower Φ values, the plasma induces stronger variations in mid-order coefficients (e.g., Z6–Z15), indicating the generation of smaller turbulent structures that contribute to flame wrinkling.
- Changes in Hu moments, particularly Hu3 and Hu5, which indicate variations in flame shape invariance and possible shifts in dominant structural features. The increase in Hu moments at lower Φ suggests a stronger departure from the original flame symmetry due to plasma-induced interactions.
- A modification of the centroid positions, particularly for lower Φ values, indicating a displacement of the reaction zone, likely due to plasma-induced flow modification. At $\Phi = 0.58$ and $\Phi = 0.45$, the centroid shift is more pronounced, suggesting a redistribution of the reaction zones, likely caused by enhanced local mixing and flame stretching effects.
- Alterations in flame curvature and perimeter, which suggest modifications in the local flame front wrinkling and overall length scale of turbulent structures. The increase in mean curvature at lower Φ values under plasma actuation suggests enhanced local flame stretch effects, particularly noticeable in the OH* emission.

In Fig. 4, OH* emission exhibits stronger variations in curvature and centroid shift, indicating that the flame front is more affected by plasma-induced instabilities than the bulk heat release region. This is further confirmed by the variation in the first few Zernike modes (Z2–Z5), which are more sensitive to large-scale shape changes, demonstrating that OH* is more susceptible to perturbations introduced by plasma.

The results indicate that plasma actuation influences both the global and local flame structure, altering its symmetry and reaction zone distribution. The observed variations in shape descriptors are consistent with the dynamic flame behavior analyzed in the subsequent spectral and modal decomposition studies. In particular, the redistribution of energy across POD modes correlates with the changes in Zernike and Hu descriptors, reinforcing the interpretation that plasma modifies the spatial organization of the flame.

The increased asymmetry observed under plasma actuation should not be interpreted independently as either a stabilizing mechanism or a precursor to blowout. In the present burner, it is more likely associated with the spatially non-uniform coupling between the filamentary plasma discharge, the swirling flow and the reaction zone. This interaction locally modifies radical production, heat release and momentum transfer, promoting flame-front wrinkling and localized redistribution of the reaction zone. Consequently, although the instantaneous flame shape becomes less axisymmetric, this behavior is accompanied by a reduced lift-off height, stronger flame anchoring near the injector, lower downstream OH* variance and attenuation of selected large-scale coherent oscillations. Under the investigated operating conditions, these observations indicate that the plasma primarily suppresses large-scale flame motions while allowing localized geometric irregularities associated with the plasma–flow interaction. Therefore, flame asymmetry alone is not adopted here as an indicator of either improved stability or incipient blowout, but should be interpreted together with the complementary spatial and dynamic diagnostics.

To facilitate the physical interpretation of the radar charts, Table 2 summarizes the percentage variation of representative Zernike descriptors together with the first Hu invariant moment (Hu1) and the mean flame-front curvature under plasma actuation. Positive percentage variations denote an increase of the corresponding descriptor under plasma actuation, whereas negative values indicate a reduction. Since the descriptors quantify different geometric characteristics of the flame, the sign of the variation should be interpreted according to the physical meaning of each parameter rather than as an intrinsic improvement or deterioration of flame behaviour.

Lower-order Zernike moments primarily characterize the global flame geometry, including axisymmetry and ellipticity, whereas higher-order moments become progressively more sensitive to boundary deformation and localized flame-front irregularities. Hu1 provides complementary information on the overall compactness of the flame, while the mean curvature quantifies the average flame-front corrugation.

The quantitative analysis indicates that plasma actuation modifies the flame morphology in a condition-dependent manner. In particular, Hu1 increases consistently for all investigated equivalence ratios (+34.2%, +25.9% and +10.8% for $\Phi = 1$, 0.8 and 0.58, respectively), indicating a progressively more compact flame structure under plasma actuation. Similarly, the representative Zernike descriptors exhibit different responses depending on the operating condition, demonstrating that plasma redistributes the relative contribution of the various geometric modes rather than producing a uniform modification of flame symmetry or boundary deformation.

The mean flame-front curvature further supports this interpretation. At $\Phi = 1$, plasma actuation increases the average curvature by approximately 53%, suggesting enhanced local flame-front deformation associated with the stronger interaction between the plasma discharge and the attached flame. Conversely, under leaner conditions ($\Phi = 0.8$ and 0.58), the mean curvature decreases by approximately 6% and 5%, respectively, indicating a smoother flame front as plasma suppresses large-scale flame oscillations approaching lean blowout. These observations are fully consistent with the POD analysis and the reduction of coherent flame dynamics discussed in the previous sections.

3.2.3. *Modal decomposition analyses*

To better understand the impact of sinusoidal plasma discharge on combustion enhancement, two POD-based methods are utilized to discern the coherent structures and energetic modes within the flame.

Since the modal energy distributions are obtained from a finite number of snapshots, a bootstrap resampling procedure was applied to quantify the statistical uncertainty associated with POD and SPOD results. For the POD analysis, 1000 bootstrap realizations were generated by randomly resampling the available OH* chemiluminescence images

Table 2
Representative variations of Zernike descriptors, Hu invariant moments and mean curvature induced by plasma actuation.

Descriptor	Physical Interpretation	Δ (%) (Plasma OFF vs Plasma ON)		
		$\Phi = 1$	$\Phi = 0.8$	$\Phi = 0.58$
Z20	Global axiaymmetry	−18.9%	−31.2%	−4.6%
Z22	Ellipticity	−40.4%	+31.0%	+0.2%
Z40	Overall flame morphology	+30.9%	−33.8%	+4.8%
Z42	Boundary deformation	−15.4%	−25.9%	−1.8%
Z44	Higher-order flame-front irregularities	+16.8%	+1.7%	+10.5%
Hu1	Global compacteness	+34.2%	+25.9%	+10.8%
Mean Curvature	Flame-front corrugation	+52.6%	−6.0%	−4.7%

with replacement. The 95% confidence intervals were calculated from the 2.5th and 97.5th percentiles of the resulting distributions. Similarly, for SPOD, the uncertainty of the first energetic mode was evaluated for each frequency interval by resampling the available spectral blocks. The corresponding confidence intervals are reported as error bars in Figs. 5 and 6.

Fig. 5 provides a detailed view of the relative energy captured by the first 8 POD eigenmodes (fluctuations) for OH* radicals, both with and without plasma discharges. Notably, these modes represent a significant portion of the relative energy. In particular, Mode 1 of the POD captures the most significant energetic structures in the flame dynamics by representing the highest variance in the dataset. This mode highlights the dominant fluctuations in the flow, which often correlate with areas of higher instability. The use of plasma actuation reduced heat fluctuations in Modes 1-8, as underlined by the decreased energy content. This is in agreement with the findings of other works [58].

At $\Phi = 1$, the fuel-air mixture is at its most efficient, resulting in higher combustion temperatures and more complete combustion. This leads to strong, coherent flame structures that dominate the flame dynamics, making the flame naturally more stable. Consequently, the energy of these dominant structures is primarily captured in the first mode, leading to a high relative energy for mode 1, as shown in Fig. 5.

The reduction in the relative energy of mode 1 with plasma indicates that the plasma discharges are causing the energy to spread to higher modes. This occurs because plasma helps suppress larger-scale dominant flame structures and generates smaller, more numerous structures, distributing the stabilization more evenly and reducing the dominance of any single mode.

Without plasma, at lower equivalence ratios, the energy is more dispersed due to higher instability and turbulence. With plasma, the stabilization effect reduces large-scale instabilities and enhances reaction rates, causing still a redistribution of energy across modes and reducing the relative energy of mode 1. However, this indicates a more stable and evenly distributed flow field, enhancing overall combustion stability. Moreover, the presence of energy observed in the first mode for OH* radicals at the lowest equivalence ratio $\Phi = 0.45$, where plasma is ON, suggests that plasma is intensifying combustion reactions in a very localized area, particularly near the nozzle exit. This localization implies that OH* radicals are predominantly generated in this confined zone, likely due to plasma enhancing the breakdown of fuel and initiating partial combustion reactions more effectively at this point. The POD energy distribution indicates that the plasma's influence is primarily focused on stabilizing and maintaining the initial stages of combustion. This results in a lack of smaller, more distributed combustion structures further along the flame, as the plasma's effects do not extend sufficiently to support the development of these structures. Essentially, the plasma ensures the flame remains stable and anchored at the critical ignition point but does not promote the spread of energy that would facilitate a more complex and evenly distributed flame structure, as evidenced by the POD images in the subsequent figures.

The relative energy captured by Mode 1 is examined in terms of frequency ranges based on the SPOD analysis. In this case, Mode 1 of the SPOD captures the most energetic mode in terms of frequency dynamics, typically associated with low-frequency behavior, which corresponds to the mean flame dynamics. Fig. 6 provides a comprehensive spectral analysis of the energy content associated with Mode 1 for OH* radicals, comparing the test cases in the presence of plasma actuation with the ones in the absence of plasma. It is evident that the energy concentrations in both cases (in the presence and in the absence of actuation) exhibit a predominant peak in the frequency range 15.6 Hz – 31.3 Hz within the low-frequency range. Nevertheless, the introduction of plasma actuation leads to a reduction in energy intensity within the low-frequency range. Without actuation, the energy spectra demonstrate a notable peak in intensity within the high-frequency range, specifically around the frequency range 313 Hz – 328 Hz and 484 Hz - 500 Hz under lean conditions ($\Phi = 0.8$ and 0.58, respectively).

When employing plasma actuation, the energy peak is absent in the case of $\Phi = 0.8$ and $\Phi = 0.58$. However, in the case of $\Phi = 0.45$ (in which one the flame is present only in the presence of actuation), the energy intensity peak remains in the frequency range 15.6 Hz - 150 Hz.

When considering higher Φ values, it is evident that peaks at lower frequencies carry greater significance in terms of relative energy compared to those at higher frequency ranges.

Figs. 7 and 8 show the POD and SPOD modes of OH* chemiluminescence images at two different Φ conditions, with and without plasma actuation. The contour plots illustrating the mode shapes exhibit variability in their scale and sign, influenced by individual time coefficients. This adaptability arises from the adjustment of plots based on the specific temporal characteristics associated with each mode shape.

Moreover, the use of red and blue hues serves to accentuate regions

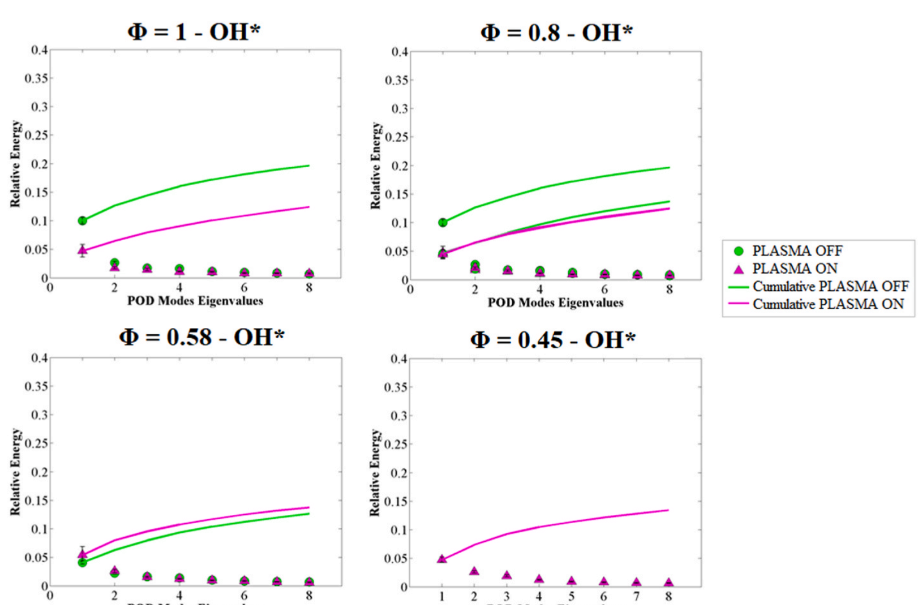

Fig. 5. Relative and cumulative energy contributions of the first eight POD modes extracted from OH* chemiluminescence images for $\Phi = 1$, 0.8, 0.58, and 0.45, with plasma OFF and ON. Error bars indicate the 95% confidence intervals estimated through bootstrap resampling of the temporal POD coefficients.

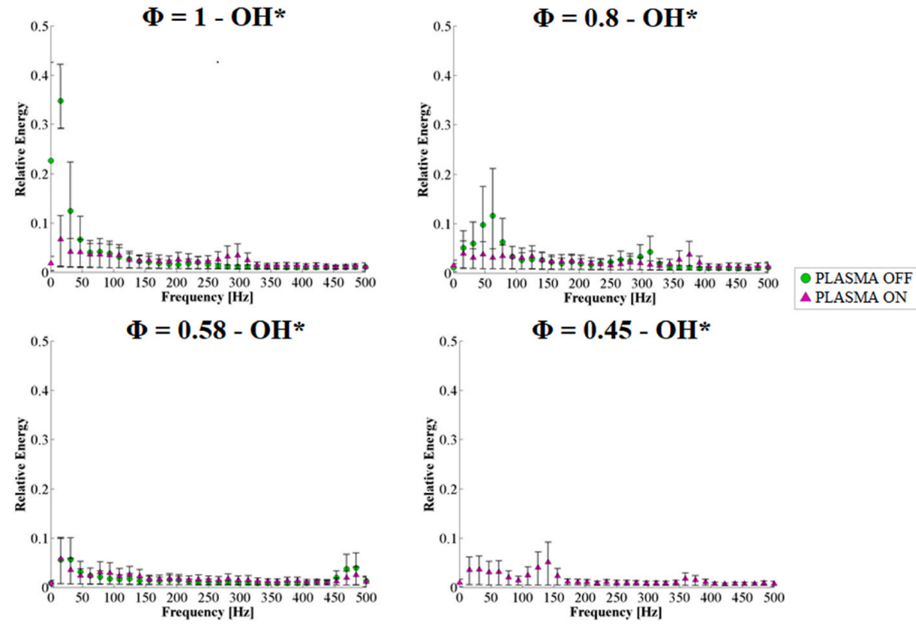

Fig. 6. Percentage of energy content of the first SPOD mode over the analyzed frequency range of OH* chemiluminescence images for operating conditions at $\Phi = 1$, 0.8, 0.58, and 0.45. Error bars indicate the 95% confidence intervals evaluated through bootstrap analysis.

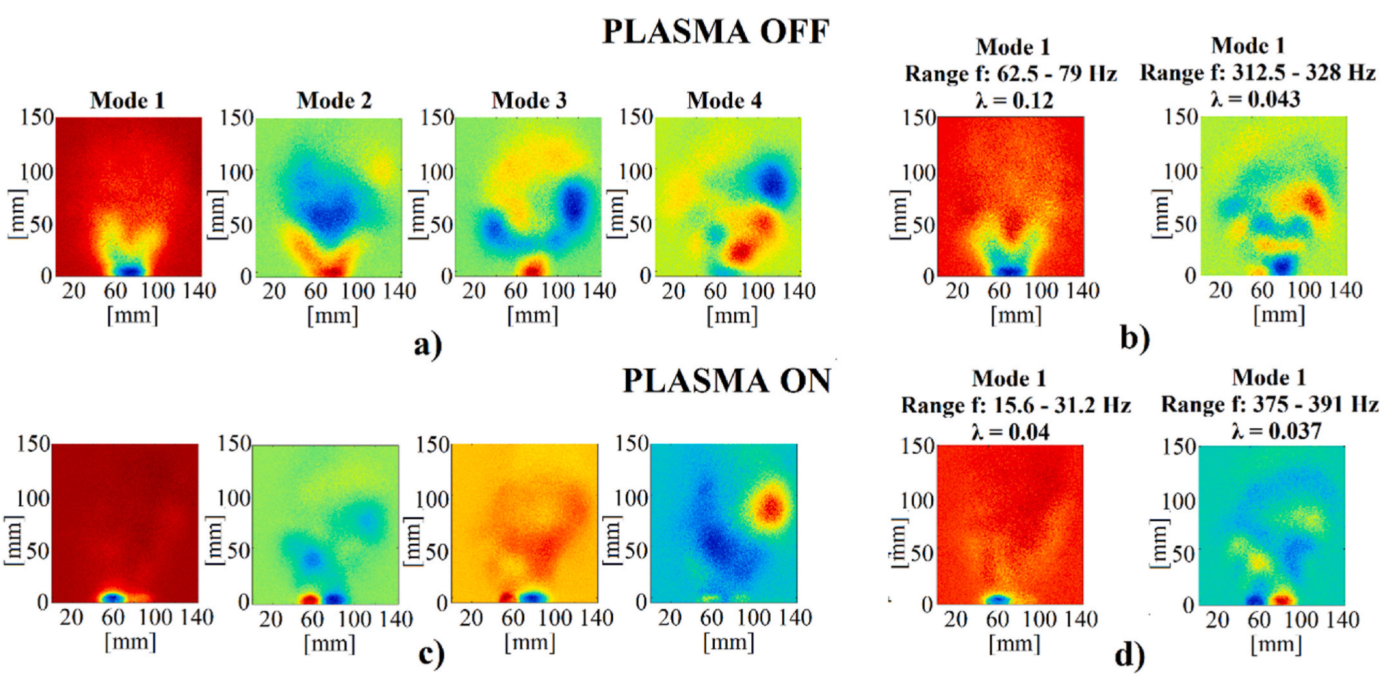

Fig. 7. Comparative analyses of POD (a-c) and SPOD (b-d) of OH* chemiluminescence images at $\Phi = 0.8$: a) and b) with Plasma OFF and c) and d) with Plasma ON.

characterized by the most pronounced fluctuations in intensity. The choice of these colors is not arbitrary; rather, it imparts meaningful information about the dynamic behavior of the system. The employment of red and blue carries additional significance, as these colors symbolize opposing directions of change within the mode shapes. This contrast in colors is not merely aesthetic but serves as a visual cue indicating a notable phase difference of π (pi) between distinct zones. In simpler terms, as one region reaches its peak intensity, the counterpart manifests its trough, underscoring a precise and systematic phase shift of 180°. This intentional use of colors and scaling methodologies enriches the visual representation, offering a nuanced understanding of the intricate relationships and fluctuations within the mode shapes.

Higher modes reveal distinct coherent structures important for investigating flame stability. With increasing mode numbers, the wavenumber of this motion and the frequency linked to the corresponding flow field (fluctuations) also increase.

The POD and SPOD analysis demonstrate that the spatial modes consist of symmetric disturbance and asymmetric disturbance that presents as global oscillation and as rotational perturbation in inner shear layer, respectively.

Fig. 7 illustrates the POD and SPOD modes of OH* chemiluminescence images without plasma actuation (Fig. 7a and b respectively) and in the presence of plasma actuation (Fig. 7c and d respectively) at $\Phi = 0.8$.

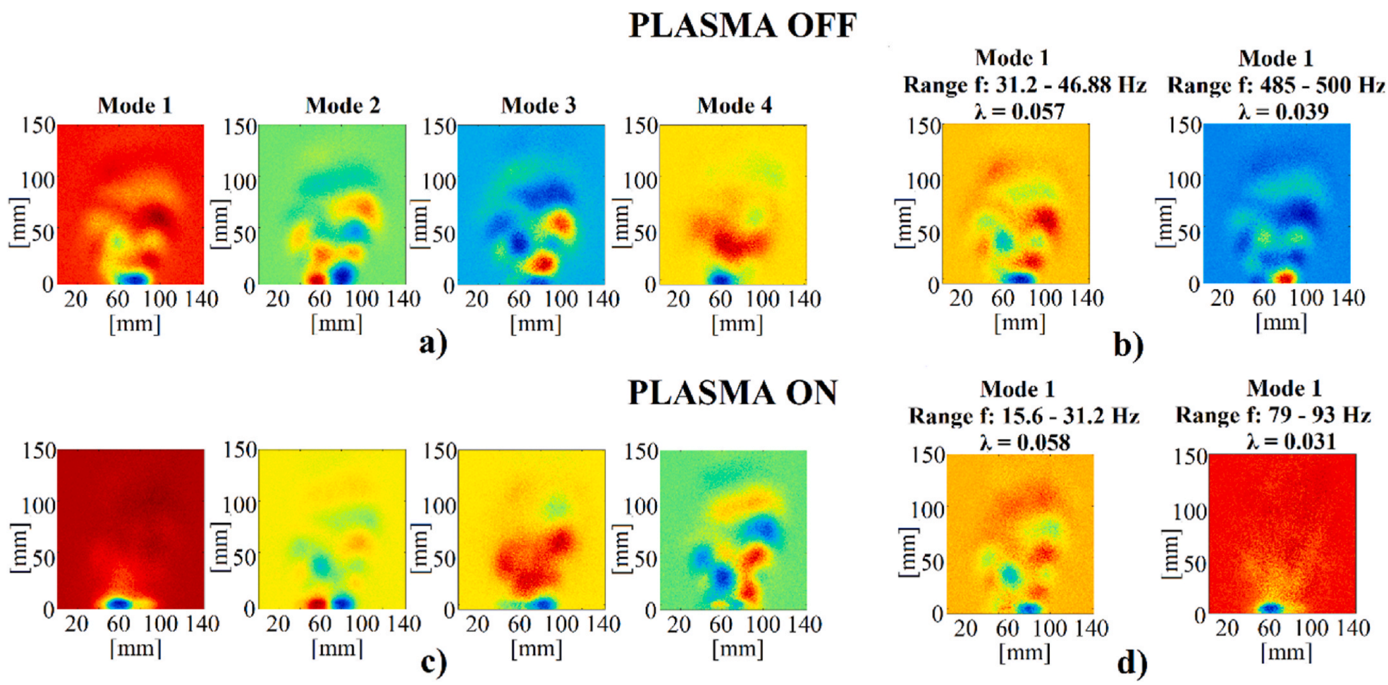

Fig. 8. Comparative analyses of POD (a-c) and SPOD (b-d) of OH* chemiluminescence images at $\Phi = 0.58$: a) and b) with Plasma OFF and c) and d) with Plasma ON.

In this first operating condition, the plasma-off configuration is characterized by a highly energetic first mode ($\lambda = 0.12$), concentrated at the flame base and extending vertically along the symmetry axis. This mode, associated with the frequency range of 62.5–79 Hz, suggests the presence of large-scale coherent structures aligned with the jet flow, possibly related to buoyant and shear-driven instabilities. The higher modes (Modes 2–4) exhibit symmetric patterns and lateral structures, indicative of vortical dynamics in the shear layers and mixing zones.

When plasma is activated, the structure of the dominant SPOD mode becomes markedly more compact and localized at the flame root. The energy of this mode drops significantly to $\lambda = 0.04$, and its spectral content shifts to lower frequencies (15.6–31.2 Hz), suggesting that plasma suppresses the large-scale instabilities that drive long-range coherence. This contraction of coherent energy and frequency downshift is consistent with a more stable and anchored flame, likely due to enhanced reactivity and heat release near the injector induced by plasma-assisted chemistry. The spatial distribution of higher modes also becomes less structured and more spatially confined, indicating an overall reduction in the complexity and extent of fluctuating dynamics.

Fig. 8 illustrates the POD and SPOD modes of OH* chemiluminescence images without plasma actuation (Fig. 8a and b respectively) and in the presence of plasma actuation (Fig. 8c and d respectively) at $\Phi = 0.58$.

In this second operating condition, the plasma-off case shows a moderately energetic first mode ($\lambda = 0.057$) that extends from the flame base upward with asymmetrical lateral features. This suggests a more irregular and unstable flame, with energy distributed across multiple coherent structures. The higher-order modes present complex spatial features associated with lower-energy flame-front fluctuations and small-scale oscillatory components. The spectral content of the most energetic mode is centered in the 31.2–46.88 Hz band.

When plasma is introduced in this condition, the first mode remains localized at the flame base and retains a similar energy level ($\lambda = 0.058$), but a redistribution of energy across frequency bands becomes evident. Notably, plasma dampens the structures in the higher frequency range (79–93 Hz), where λ drops to 0.031. Furthermore, the spatial complexity of higher modes (Modes 2–4) is reduced, and their energy appears more fragmented, again indicating a stabilizing effect, albeit less pronounced than in the first case. This suggests that under richer or higher-load conditions, plasma is still capable of modulating flame dynamics, but its relative influence on dominant coherent structures may be lower.

Overall, the SPOD results demonstrate that NTPAC significantly alters the spectral and spatial characteristics of flame dynamics, particularly by attenuating low-frequency coherent structures and confining their spatial extent. This effect is especially evident under leaner or less stable conditions. The observed reduction in modal energy and simplification of dominant patterns support the hypothesis that plasma enhances flame stabilization through localized reactivity enhancement, as corroborated by time-averaged chemiluminescence fields and geometric flame parameters.

POD and SPOD provide complementary descriptions of the flame dynamics. POD ranks the dominant spatial structures according to their contribution to the total fluctuation energy over the entire acquisition; however, each POD mode may contain several oscillatory components occurring at different frequencies. In contrast, SPOD performs the decomposition in the frequency domain through the cross-spectral density matrix, thereby isolating spatially coherent structures associated with individual spectral bands. This distinction is particularly relevant in plasma-assisted combustion, where plasma actuation modifies flame dynamics through a frequency-dependent redistribution of coherent structures rather than a uniform attenuation of fluctuations.

The comparison between the POD temporal coefficients and the corresponding SPOD modes demonstrates the additional insight provided by the spectral decomposition. While POD identifies the dominant energetic structures governing the global flame response, SPOD determines the characteristic frequencies at which these structures evolve, enabling changes in modal energy, spatial localization, spectral content and coherence induced by plasma actuation to be identified separately.

To facilitate this comparison, Table 3 summarizes the dominant modal characteristics for the investigated operating conditions. The table highlights how POD captures the global energetic organization of the flame, whereas SPOD resolves the same coherent structures within their corresponding frequency bands. The combined interpretation demonstrates that plasma primarily redistributes coherent flame dynamics across the frequency spectrum, revealing stabilization mechanisms that cannot be inferred from the conventional POD energy ranking

Table 3
Systematic comparison between POD and SPOD results for the investigated operating conditions.

Operating condition	POD Interpretation	SPOD Dominant frequencies	SPOD Interpretation	Plasma effect
Φ = 0.80, Plasma OFF	MODE 1 – Global axial mode	**62.5–79 Hz** (λ ≈ 0.12)	Extended coherent structure	Baseline condition
Φ = 0.80, Plasma ON	MODE 1 – Weaker global mode	**15.6–31.2 Hz** (λ ≈ 0.04)	Localized flame-root structure	67% modal energy reduction; frequency downshift
Φ = 0.58, Plasma OFF	MODE 1 – Asymmetric global mode	**31.2–46.9 Hz** (λ ≈ 0.057)	Extended asymmetric structure	Baseline near-LBO reference dynamics
Φ = 0.58, Plasma ON	MODE 1 – Modal energy redistribution	**31.2–46.9 Hz** (λ ≈ 0.058)	Localized coherent structure	High-frequency damping; reduced spatial complexity

alone.

3.3. *Time-frequency analysis of flame structures*

This section examines the time-frequency analysis of the POD and SPOD modes from chemiluminescence images to understand the dominant modes affecting flame dynamics. Techniques like FFT, wavelet transforms, phase portraits, and autocorrelation are used to decompose the non-stationary signals of these modes into their constituent frequencies over time, revealing their temporal and spectral characteristics.

The results enhance the understanding of the temporal evolution of combustion modes and help identify key dynamic features such as periodicities, growth rates, and damping mechanisms in the flow dynamics. High-frequency plasma discharges (20 kHz) improve combustion kinetics by stabilizing the flame and mitigating low-frequency oscillations, reducing blowout risks. Since the OH* chemiluminescence images were acquired at 1000 Hz and the corresponding Nyquist frequency is 500 Hz, this study focuses on the lower frequency range (1-500 Hz), aligning with previous research that identifies critical instability frequencies near blowout conditions in methane-air flames.

Research by Bompelly et al. [59], Thampi and Sujith [60], and others have noted key instability frequencies in methane-air flames near blowout conditions primarily exist within the range 0-100 Hz. The frequency observations include:

- Low-frequency oscillations typically observed in the range of 1 - 20 Hz, associated with large-scale pulsations and global flame movements, as discussed in Santhosh and Basu [61].
- Intermediate-frequency oscillations found in the range of 20 - 100 Hz, related to hydrodynamic instabilities and vortex shedding phenomena, highlighted by Nair and Lieuwen [62].
- High-frequency oscillations observed in the range of 100 - 300 Hz, related to acoustic modes and finer-scale turbulent interactions, as noted in the work by Xi et al. [63] and Zhen et al. [64].

Acoustic measurements using a high-temperature microphone probe complement the analysis of combustion dynamics through POD and SPOD of chemiluminescence images, offering a comprehensive view of how plasma influences both the visual and acoustic characteristics of the flame. The study correlates changes in sound pressure levels with flame structure and instability variations observed in POD/SPOD modes.

The acoustic and OH* imaging measurements were not acquired using a common synchronization signal. Therefore, the comparison between their spectra is limited to the identification of common frequency ranges. No magnitude-squared coherence, cross-phase, or Rayleigh-index analysis can be performed reliably from the present datasets, and the observed spectral correspondence should not be interpreted as direct evidence of phase-resolved thermos-acoustic coupling.

As shown in Fig. 9, the comparison of PSD from microphone signals and OH* POD mode coefficients at Φ = 0.58 with and without plasma actuation shows that plasma significantly impacts the frequency of fluctuations, which can be linked to heat transfer. Distinct dominant frequencies emerge when comparing tests with and without plasma activation.

To quantitatively assess the variations in sound pressure levels between the swirl and plasma-stabilized cases, acoustic measurements are also conducted by using a high-temperature probe microphone. Particularly, it is noticed that when operating in the presence of plasma actuation, the flame exhibits a robust attachment to the nozzle exit, accompanied by a noticeable reduction in the associated noise level.

Results show that the presence of plasma has a notable influence on the frequency of fluctuations observed in both the acoustic signal and POD modes, which can be qualitatively linked to heat transfer. Clearly, distinct frequencies emerge as dominant within the combustor when comparing tests with and without plasma activation. This behavior indicates that plasma actuation modifies the distribution of fluctuation energy among the dominant oscillatory structures rather than simply suppressing all frequency components.

By decreasing the fuel/air ratio to Φ = 0.58, the predominant frequency peaks in the acoustic signals emerge at 252 Hz and approximately 460-490 Hz. Notably, this latter frequency range is observable in the power spectrum of the initial two POD modes of OH* chemiluminescence signals.

When plasma control is applied, there is a decrease in the energy content of the microphone signal spectrum, as indicated by the area under the PSD. This implies that the flame exhibits reduced oscillations and achieves greater stability. In essence, the implementation of plasma control helps mitigate flame fluctuations, resulting in a more robust and controlled behavior. The implementation of plasma discharges notably decreases the amplitude of peaks, particularly within the [400-500 Hz] range, although this attenuation is accompanied by a redistribution of spectral energy toward other frequency components. Additionally, the peak shifts in the frequency range [469-484 Hz].

Although the attenuation of low-frequency spectral components becomes less pronounced at Φ = 0.58, this behavior should not be interpreted as a reduction of the plasma stabilization effectiveness. Near the lean blowout limit, plasma-generated reactive species and localized energy deposition primarily contribute to sustaining flame anchoring and combustion chemistry rather than uniformly suppressing all low-frequency oscillations. Consequently, the stabilization mechanism progressively shifts from attenuation of dominant coherent oscillations toward maintenance of a bounded and attached flame despite the persistence of low-frequency dynamical responses.

The frequency analysis indicates that plasma actuation does not uniformly suppress all modal and spectral components. Instead, the discharge modifies the distribution of fluctuation energy among the dominant POD structures, with attenuation of selected intermediate- and high-frequency components and possible amplification of specific low-frequency contributions depending on the operating condition. Therefore, the plasma effect is interpreted as a mode- and frequency-dependent reorganization of the flame dynamics rather than as a broadband suppression of oscillations. The stabilization effect is assessed through the combined analysis of spectral characteristics, acoustic fluctuation amplitude, flame anchoring behavior and complementary OH* diagnostics.

When analyzing the total area under the FFT curve, a clearer trend emerges across the equivalence ratios. At Φ = 0.58 without plasma, the

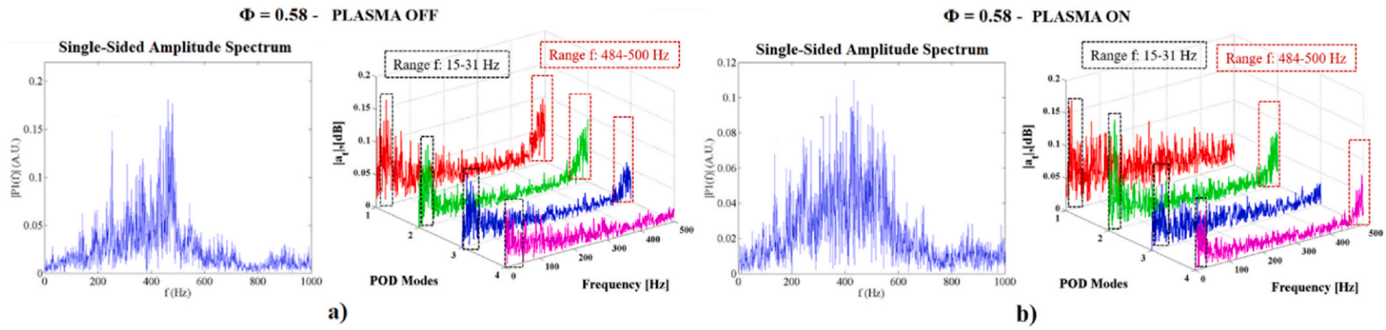

Fig. 9. Power spectral density of microphone signal (on the left) and of the time coefficients of POD modes of OH* chemiluminescence images (on the right) for the case at $\Phi = 0.58$: a) with Plasma OFF and b) with Plasma ON.

area is 33.45 (0-10,000 Hz) and 24.97 (0-1000 Hz), while with plasma it increases to 47.33 and 22.94, respectively.

This increase in total area indicates greater overall energy in the flame's frequency response, signifying more substantial fluctuations and instabilities. These findings align with the higher variance observed in the POD analysis.

Fig. 10 shows the histograms of the wavelet energy contents of the microphone signals at ambient temperature at different Φ values, with and without plasma actuation.

The point to highlight is the consistency of the signals acquired with the microphone with the POD and SPOD analyses applied to the chemiluminescence images. It should be emphasized that, in the presence of plasma, the energy content increases or decreases within specific frequency ranges. Specifically, in the presence of plasma, there is an increase in the range [0-78.125 Hz] for all equivalence ratios. However, in the proximity of blowout, the-frequency content in the range [156.25Hz-312.5Hz] decreases at $\Phi = 0.58$ and $\Phi = 0.45$ when using plasma discharge.

At $\Phi = 1$ and $\Phi = 0.8$, the distributions exhibit the most significant energy contribution within the ranges [78.125Hz −156.25Hz] and [156.25Hz-312.5Hz]. This pattern persists in the presence of plasma actuation. However, in the latter scenario, the wavelet energy within the [156.25Hz-312.5Hz] range decreases due to plasma discharges. Under lean fueling conditions ($\Phi = 0.58$), the wavelet energy in the [78.125Hz −156.25 Hz] range increases without actuation compared to the conditions at $\Phi = 1$ and $\Phi = 0.8$. When applying plasma actuation, the energy in this range decreases to a level comparable to the highest Φ, indicative of a stable flame.

Fig. 11 presents a series of phase portraits for the first, second, and third POD modes (1 vs 2, 2 vs 3, 3 vs 4) of OH* radicals. Each portrait captures the dynamic oscillatory The circular patterns observed across different modes indicate periodic or cyclic modal dynamics. However, the present unsynchronized measurements do not allow these oscillations to be attributed unambiguously to thermo-acoustic coupling, vortex shedding, or another specific mechanism. The variation in point spread and distribution density reflects differences in energy levels, instability intensities, and mode interactions within the combustion process. The unit of measurement is arbitrary because these coefficients are normalized during the decomposition process. Their values are relative and do not represent physical quantities with standard units, but rather the contribution or "energy" of each mode at a given time.

A $\Phi = 0.8$ the ellipticity appears to be more pronounced in the phase portraits where plasma is active ("Plasma ON") than when it is deactivated ("Plasma OFF"). The portraits show a more stretched or elongated distribution of data points along one axis. This observation may initially seem counterintuitive, considering plasma's role in stabilizing combustion processes. However, this ellipticity, and the dynamics it represents, can be explained through the enhanced mixing and modification of flow fields induced by plasma activation.

When plasma is on, the induced electrical fields and associated body forces can generate more vigorous local turbulence and alter the flow patterns [28] [55]. This enhancement in mixing does not simply lead to a more stable system but can introduce complex interactions between different flow scales and combustion dynamics. The increased ellipticity in the phase portraits likely reflects these complex dynamical behaviors, where multiple frequencies or modulations interact more significantly due to the altered flow conditions driven by the plasma. Moreover, the introduction of plasma leads to changes in chemical kinetics by providing additional ionization pathways or altering the concentration of reactive species. These changes can further contribute to the observed differences in the phase portraits by affecting how the flame front propagates and interacts with the flow field.

Finally, when plasma is activated, the energy and momentum it introduces can disrupt regular oscillatory patterns that are typical of certain combustion instabilities. This disruption can be visualized as an

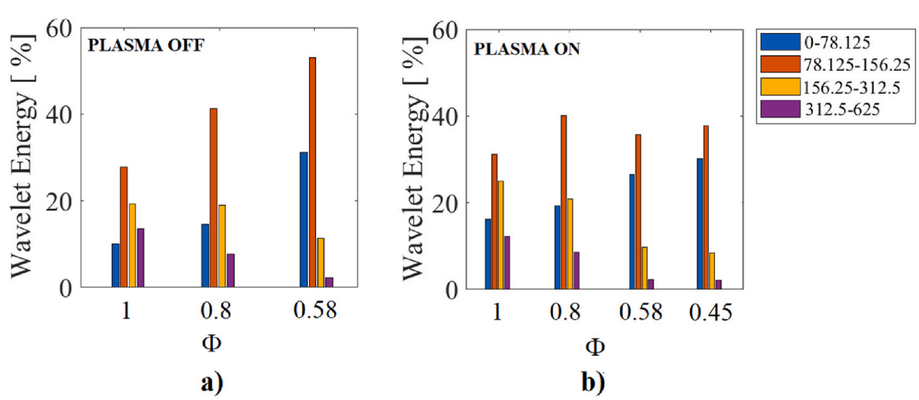

Fig. 10. Wavelet Energy comparison for different Φ values: a)with Plasma OFF actuation and b) with Plasma ON actuation.

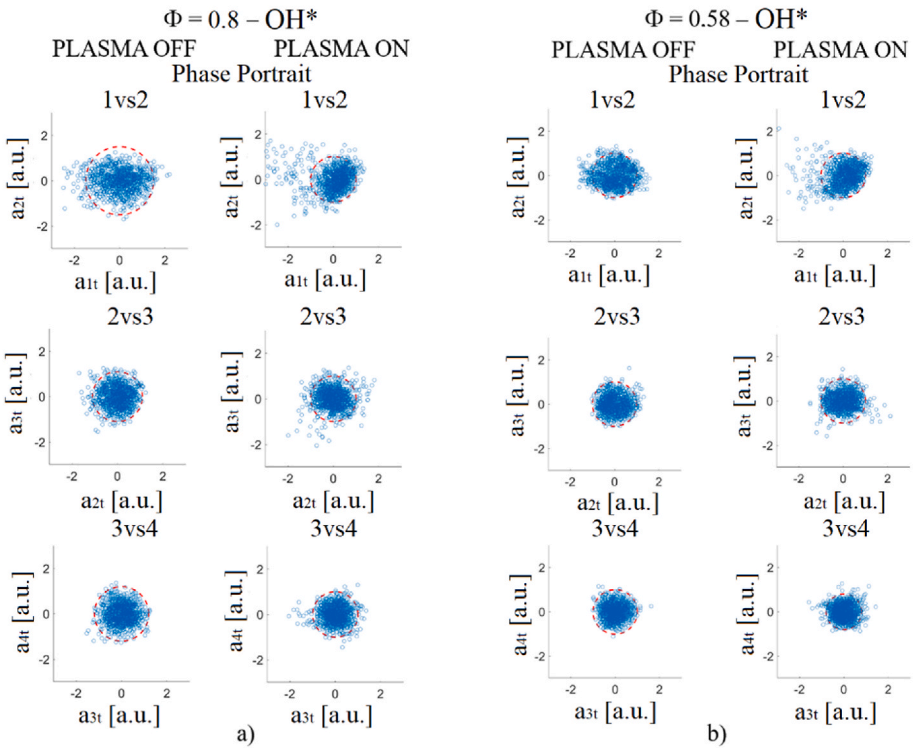

Fig. 11. Phase Portrait of the first 4 eigenvalues of the POD for OH* chemiluminescence emission: a) $\Phi = 0.8$ with Plasma OFF and ON actuation and b) $\Phi = 0.58$ with Plasma OFF and ON actuation.

increased ellipticity in the phase portraits, which suggests less regularity and a more complex dynamic interaction within the flame.

Regular cyclic behavior may be associated with different physical mechanisms in reacting flows. In the present experiments, the reduced periodicity observed under plasma actuation indicates a reorganization of the dominant modal dynamics. Since the acoustic and OH* measurements were not synchronized, this change cannot be interpreted as direct evidence of mitigation of thermo-acoustic instabilities. Hence, a decrease in regular oscillations can also imply that the flame is less prone to being locked into specific oscillation frequencies that can resonate with the physical structure of the combustion chamber or other system components, thereby reducing the risk of structural damage or efficiency losses.

The behavior at $\Phi = 0.58$ contrasts with richer mixtures (higher Φ); where increased fuel availability leads to more vigorous combustion dynamics, higher heat release, and potentially more instabilities and complex interactions. This results in a greater spread of data points in phase portraits, indicating a broader range of dynamic behaviors and instabilities as the system responds more sensitively to perturbations, as plasma discharges.

To quantitatively characterize the geometry of the modal phase portraits, the area of the 95% covariance ellipse was computed from the covariance matrix of the POD temporal coefficients. The ellipse semi-axes were obtained from the eigenvalues of the covariance matrix and scaled using the χ^2 quantile corresponding to a 95% probability level ($\chi^2_{2,0\cdot 95} = 5.991$). In addition, the ellipse aspect ratio and the RMS radius were evaluated to quantify trajectory anisotropy and spatial dispersion.

The modal phase portraits provide a qualitative representation of the temporal evolution of the dominant POD coefficients and therefore describe the organization of the reconstructed modal dynamics in phase space. Under plasma actuation, the trajectory geometry is modified, with changes in both the occupied phase-space region and the trajectory anisotropy depending on the operating condition and the modal pair considered. Quantitative evaluation based on the 95% covariance ellipse area, ellipse aspect ratio and RMS radius indicates that these changes are generally limited at $\Phi = 0.80$, whereas more pronounced modifications are observed at $\Phi = 0.58$, particularly for the dominant modal pair (a_1 vs a_2), where the ellipse area and RMS radius increase by approximately 34% and 17%, respectively. It should be emphasized that the geometric characteristics of the phase portraits cannot be interpreted as direct measures of combustion stability. Broader or more elliptical trajectories may arise from changes in modal amplitude, phase coherence or multi-frequency interactions and therefore do not uniquely indicate either stabilization or destabilization. Consequently, the phase portraits are used here to characterize plasma-induced dynamical reorganization of the dominant modal structures, while the assessment of flame stabilization is established from complementary diagnostics, including flame anchoring, lift-off behaviour, OH* fluctuation maps, acoustic spectra and POD/SPOD modal analyses. The complete set of quantitative phase-portrait descriptors for all operating conditions is reported in the Supplementary Material (Table S1).

In Fig. 12 the temporal series of OH* chemiluminescence SPOD mode data in the different frequency ranges provides a clear visualization of how plasma affects combustion dynamics under different fueling conditions. At $\Phi = 0.8$, without plasma, the oscillations are regular and pronounced, typical of stable cyclic behaviors linked to thermo-acoustic instabilities or vortex shedding. When plasma is on, these patterns are significantly disrupted, showing decreased amplitude and reduced temporal coherence. This behavior is consistent with the modified phase-space organization observed in the phase portraits, indicating a redistribution of the dominant modal dynamics under plasma actuation. This disruption suggests that plasma modifies the dominant oscillatory dynamics by reducing the persistence of phase-coherent structures. However, reduced periodicity alone cannot be considered a direct indicator of improved stability.

At the leaner condition, $\Phi = 0.58$, the plasma off condition shows less intense oscillations due to the lower energy state of the leaner mixture. With plasma activation, these oscillations are further dampened, reinforcing plasma's role in stabilizing combustion by modulating energy dynamics and reducing instabilities even in lower Φ conditions.

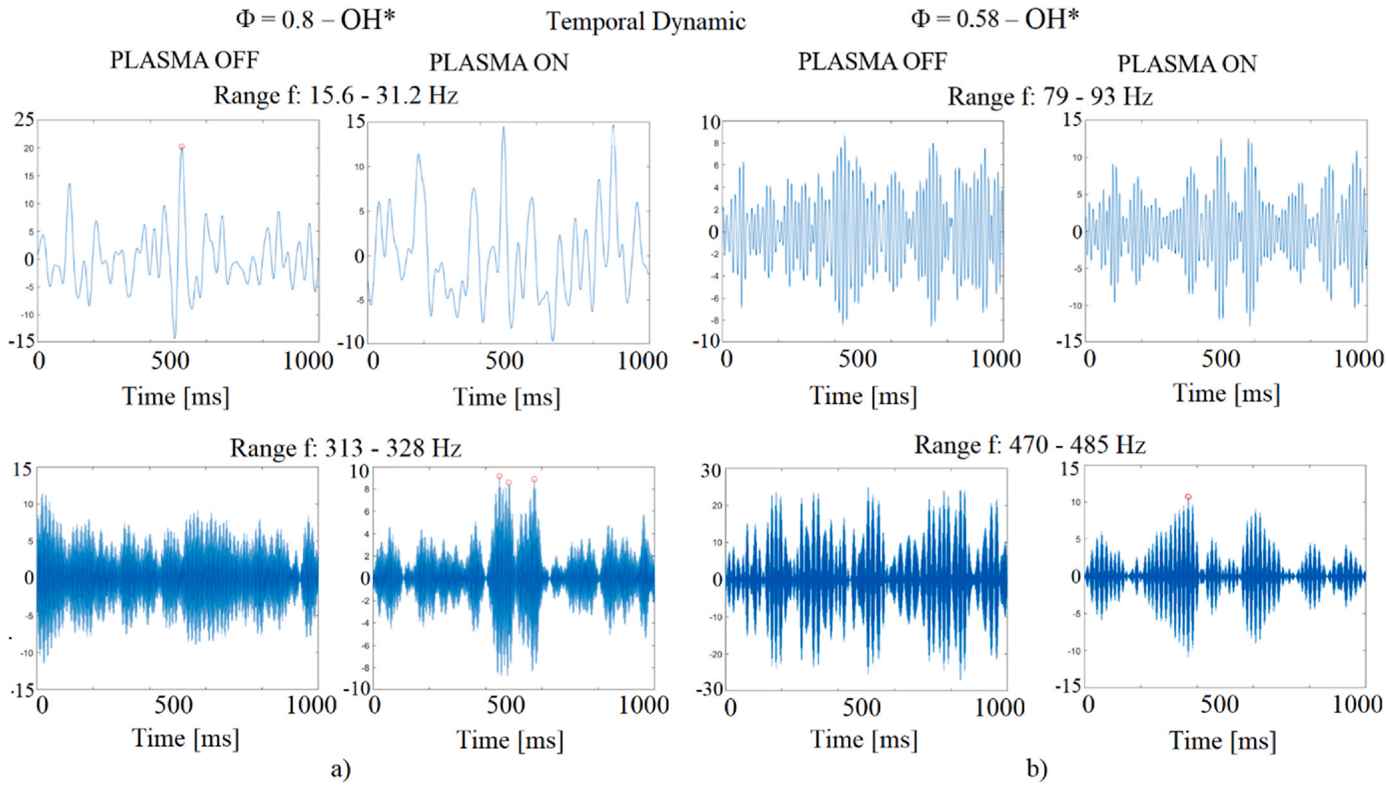

Fig. 12. Temporal Dynamics of SPOD modes: a) $\Phi = 0.8$ with Plasma OFF and ON actuation in the range of frequency equal to (15-31Hz) and (313-328 Hz) and b) $\Phi = 0.58$ with Plasma OFF and ON actuation in the range of frequency equal to (79-93 Hz) and (470-485 Hz).

This comparative analysis highlights plasma's effectiveness across different fuel/air ratios, showing a consistent pattern of reducing oscillatory amplitudes while introducing more dynamic interactions in the combustion process. The analysis of the time signals at a lower

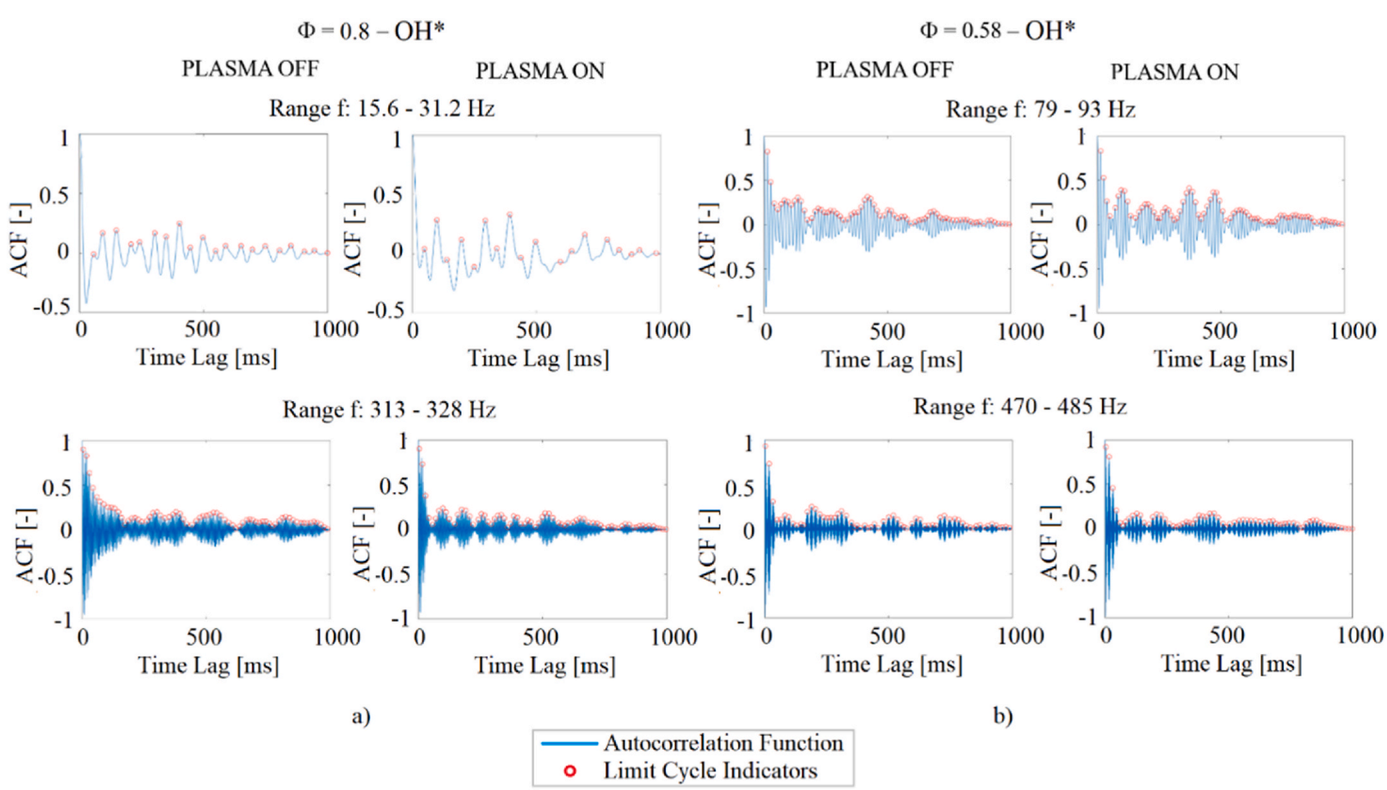

Fig. 13. Autocorrelation functions: a) $\Phi = 0.8$with Plasma OFF and ON actuation in the range of frequency equal to (15-31Hz) and (313-328 Hz) and b) $\Phi = 0.58$ with Plasma OFF and ON actuation in the range of frequency equal to (79-93 Hz) and (470-485 Hz).

equivalence ratio of $\Phi = 0.58$, particularly with plasma activation, reveals the presence of a "chugging mode," characterized by low-frequency pulsations. This phenomenon is typically observed near blowout limits and is associated with intermittent flame holding and re-ignition processes. Plasma-assisted combustion enhances these effects by intermittently stabilizing and destabilizing the flame, a behavior that is crucial under lean conditions where the risk of blowout is elevated due to reduced heat and radical production. The higher peaks observed in the time signals when plasma is active, particularly in the frequency range of 79-93 Hz, reflect plasma's dynamic interaction with the combustion process. The observed low-frequency pulsations should therefore be interpreted as a transient dynamical response associated with flame stabilization mechanisms under lean conditions, rather than as direct evidence of instability.

The autocorrelation functions, in Fig. 13, still provide a view of the impact of plasma actuation on combustion dynamics at varying Φ values and frequency ranges. For $\Phi = 0.8$, focusing on the lower frequency range (15-31 Hz), notable differences are evident when plasma is turned on and off. Without plasma, the autocorrelation function exhibits clear, periodic peaks, indicating stable and regular oscillations which are characteristic of coherent combustion structures such as large-scale vortex shedding. This stability is typical of higher fuel concentrations which support sustained oscillatory behaviors. However, when plasma discharges are introduced, these peaks diminish significantly in amplitude, and the overall autocorrelation flattens. This suggests that plasma disrupts these coherent structures, potentially by enhancing mixing or altering the local flow dynamics, leading to more chaotic or less periodic behavior.

For the same $\Phi = 0.8$ but at a higher frequency range (313-328 Hz) a similar pattern emerges. The plasma-off condition shows more distinct oscillatory behavior with clearer peaks in the autocorrelation function, indicating the presence of high-frequency instabilities or acoustic interactions within the combustion chamber. When plasma is on, these peaks are noticeably suppressed, reflecting the plasma's damping effect on these high-frequency oscillations, likely by interfering with the acoustic pathways or damping the turbulent eddies responsible for such instabilities.

Shifting to a leaner mixture at $\Phi = 0.58$ in the frequency range of 79-93 Hz, the autocorrelation functions again reveal the stabilizing role of plasma. Without plasma, the autocorrelation function shows moderate oscillatory behavior, but with plasma, this behavior is significantly muted, indicating effective plasma intervention at this intermediate frequency range, possibly through similar mechanisms of enhanced mixing and disruption of coherent structures.

At the highest frequency examined (470-485 Hz) for $\Phi = 0.58$, the autocorrelation functions under both plasma on and off conditions show less pronounced oscillatory behavior compared to lower frequencies, but with plasma on, there's a subtle but noticeable reduction in the amplitude of any oscillations present. This suggests that while plasma's effect at this high frequency is less dramatic, it still contributes to damping the finer-scale instabilities that might exist in the flame.

To further distinguish the reduction of temporal coherence from the onset of irregular unstable dynamics, additional statistical indicators were evaluated from the acoustic pressure signal. Since reduced autocorrelation peaks can be associated with both bounded stochastic fluctuations and unstable intermittent behavior, the RMS level and higher-order statistical moments were analyzed for plasma OFF and plasma ON conditions. Plasma actuation resulted in a reduction of the overall acoustic fluctuation amplitude, with the RMS value decreasing by approximately 16.9% at $\Phi = 0.80$ and 10.0% at $\Phi = 0.58$. Moreover, the kurtosis remained close to the Gaussian reference value ($\sim$3), varying from 3.08 to 3.12 at $\Phi = 0.80$ and from 2.83 to 3.07 at $\Phi = 0.58$. These results indicate that the loss of periodic coherence induced by plasma is not accompanied by an increase in large-amplitude intermittent events. Therefore, the autocorrelation analysis is interpreted as evidence of a dynamical reorganization of the flame response rather than as a standalone indicator of enhanced stability.

Overall, the autocorrelation analysis demonstrates that plasma actuation modifies the dominant oscillatory dynamics by weakening phase-coherent periodic components across different frequency ranges. When combined with the reduced acoustic fluctuation amplitude, sustained flame anchoring and the other diagnostic observations, these results indicate that plasma promotes a more controlled flame response without introducing additional large-amplitude unstable oscillations.

4. Conclusion

This work experimentally investigated the influence of sinusoidal non-thermal plasma actuation on the stabilization of lifted methane/air swirl flames operating under lean conditions. Electrical characterization, high-speed OH* chemiluminescence imaging, quantitative flame morphology analysis, modal decomposition techniques (POD and SPOD), spectral analysis, wavelet decomposition, phase portraits and acoustic measurements were combined to provide a comprehensive description of the plasma–flame interaction mechanisms.

The electrical characterization showed that the adopted sinusoidal plasma actuator operated at an average dissipated electrical power of 74 $\pm$ 8 W. Under these operating conditions, plasma actuation substantially improved flame stabilization, allowing stable combustion to be sustained down to an equivalence ratio of $\Phi = 0.45$, whereas flame blowout occurred without plasma at $\Phi = 0.58$. Time-averaged OH* chemiluminescence images further demonstrated a reduction in lift-off height and a stronger flame anchoring near the injector, while downstream OH* variance generally decreased, indicating lower large-scale flame fluctuations. The localized increase in variance observed close to the electrode was interpreted cautiously since a contribution from direct plasma emission cannot be completely excluded.

The quantitative morphological analysis demonstrated that plasma actuation modifies both the global flame geometry and the local flame-front structure. Variations of Zernike descriptors, Hu invariant moments, centroid position and mean flame curvature revealed a condition-dependent reorganization of the flame morphology rather than a uniform increase or decrease of geometric complexity. In particular, plasma generally produced a more compact flame while simultaneously promoting localized flame-front wrinkling associated with the interaction between the filamentary discharge, the swirling flow and the reaction zone. These observations indicate that the increased instantaneous asymmetry observed under plasma actuation should not be interpreted alone as an indicator of either improved or deteriorated flame stability, but rather as the consequence of localized plasma–flow coupling.

The combined POD and SPOD analyses provided complementary information on the plasma-induced modification of coherent flame dynamics. POD identified a redistribution of fluctuation energy among the dominant spatial modes, accompanied by a reduction of the contribution of large-scale coherent structures under several operating conditions. SPOD further demonstrated that this redistribution is strongly frequency dependent, allowing the dominant coherent structures to be associated with their corresponding spectral content. Plasma actuation generally reduced the spatial extent and energetic contribution of selected coherent modes while promoting a more localized flame-root dynamics. The introduction of bootstrap confidence intervals confirmed the statistical robustness of the observed modal trends despite the finite number of available snapshots.

The frequency analyses performed using POD temporal coefficients, microphone measurements and wavelet decomposition consistently indicated that plasma does not uniformly suppress all oscillatory components. Instead, it redistributes fluctuation energy among different frequency bands, attenuating selected intermediate- and high-frequency coherent structures while preserving or even enhancing specific low-frequency contributions depending on the operating condition. Consequently, the stabilization mechanism is interpreted as a frequency-dependent reorganization of flame dynamics rather than a broadband damping of combustion oscillations. Because OH* chemiluminescence and acoustic measurements were not synchronously acquired, the present results cannot be interpreted as direct evidence of thermo-acoustic coupling, and no coherence or Rayleigh-index analysis was attempted.

The results demonstrate that sinusoidal plasma actuation represents an effective strategy for extending the lean operating limit and modifying the spatial and temporal organization of lifted swirl flames. Beyond the specific combustion configuration investigated, this work also highlights the benefit of combining quantitative flame morphology descriptors with complementary POD and SPOD analyses to distinguish global energetic structures from frequency-resolved coherent dynamics. Such an integrated diagnostic framework provides a more comprehensive understanding of plasma-assisted combustion mechanisms and may support the future development and optimization of plasma-based combustion stabilization technologies for low-emission combustion systems.

Funding

This project received funding from the Clean Sky 2 Joint Undertaking (JU) under the grant agreement N. 831881 (CHAiRLIFT). The JU receives support from the European Union's Horizon 2020 research and innovation program and the Clean Sky 2 JU members other than the Union. Additional funding was provided by the European Union through the call Project HORIZON FFLECS (Grant Agreement No.101096436 - CUP F83C23003480006) -"Novel Fuel-Flexible ultra-Low Emissions Combustion systems for Sustainable aviation - FFLECS".

The author, Sara Bonuso, received funding from the Apulian Region for her PhD Fellowship.

CRediT authorship contribution statement

Sara Bonuso: Conceptualization, Data curation, Formal analysis, Investigation, Methodology, Writing – original draft, Writing – review & editing. **Ghazanfar Mehdi:** Data curation, Visualization, Writing – review & editing. **Stefan Raphael Harth:** Supervision. **Elisa Pescini:** Conceptualization, Methodology, Writing – review & editing. **Ossi Kaario:** Supervision. **Maria Grazia De Giorgi:** Conceptualization, Methodology, Supervision, Writing – review & editing.

Declaration of competing interest

The authors declare the following financial interests/personal relationships which may be considered as potential competing interests: De giorgi maria grazia reports financial support was provided by University of Salento. If there are other authors, they declare that they have no known competing financial interests or personal relationships that could have appeared to influence the work reported in this paper.

Appendix A. Supplementary data

Supplementary data to this article can be found online at https://doi.org/10.1016/j.joei.2026.102685.

References

[1] D. Wei, H. Li, H. Fang, H. Zhou, H. Li, H. Liu, X. Hu, H. Zhang, Analysis of thermoacoustic instability and emission behaviors of lean premixed biogas/ammonia flame, J. Energy Inst. 118 (2025) 101923, https://doi.org/10.1016/j.joei.2024.101923.

[2] W. Luo, W. Ding, J. Du, Y. Wang, Chemiluminescence-based control for low-emission combustion in a rich–lean staged burner, J. Energy Inst. 124 (2026) 102397.

[3] J.C. Wollgarten, N. Zarzalis, F. Turrini, A. Peschiulli, Experimental investigations of ion current in liquid fuelled gas turbine combustors, Int. J. Spray Combust. Dyn. 9 (2017) 172–185.

[4] G. Sarras, Y. Mahmoudi, L.D. Arteaga Mendez, et al., Modeling of turbulent natural gas and biogas flames of the Delft jet-in-hot-coflow burner: effects of coflow temperature, fuel temperature and fuel composition on the flame lift-off height, Flow Turbul. Combust. 93 (2014) 607–635.

[5] S.B. Leonov, S. Elliott, C. Carter, A. Houpt, P. Lax, T. Ombrello, Modes of plasma-stabilized combustion in cavity-based M = 2 configuration, Exp. Therm. Fluid Sci. 124 (2021) 110355.

[6] R.J. Dijoud, N. Laws, C. Guerra-Garcia, Mapping the performance envelope and energy pathways of plasma-assisted ignition across combustion environments, Combust. Flame 271 (2025) 113793.

[7] A. Morales, T. Genova, J. Reyes, I. Boxx, K. Ahmed, Turbulence-driven blowout instabilities of premixed bluff-body flames, Flow Turbul. Combust. 108 (2021), https://doi.org/10.1007/s10494-021-00269-8.

[8] G. Mehdi, S. Bonuso, M.G. De Giorgi, Effects of nanosecond repetitively pulsed discharges timing for aeroengines ignition at low temperature conditions by needle-ring plasma actuator, Energies 14 (2021) 5814.

[9] G. Mehdi, M.G. De Giorgi, D. Fontanarosa, S. Bonuso, A. Ficarella, Ozone production with plasma discharge: comparisons between activated air and activated fuel/air mixture, in: Proceedings of the ASME Turbo Expo 2021, 2021. Paper No. GT2021-60167.

[10] D. Fontanarosa, G. Mehdi, M.G. De Giorgi, A. Ficarella, Assessment of the impact of nanosecond plasma discharge on the combustion of methane-air flames, E3S Web of Conferences 197 (2020) 10001.

[11] Z. Wang, B. Aravind, S. Mashruk, A. Valera-Medina, Numerical investigation on the combustion characteristics of premixed NH3-air flames using gliding arc plasma, J. Energy Inst. 123 (2025) 102314, https://doi.org/10.1016/j.joei.2025.102314.

[12] E. Pescini, D.S. Martínez, M.G. De Giorgi, A. Ficarella, Characterization of the effects of a dielectric barrier discharge plasma actuator on a coaxial jet in a Bunsen burner, Exp. Therm. Fluid Sci. 91 (2018) 292–305.

[13] J. Sun, Y. Bao, K. Zhang, A.A. Konnov, M. Richter, E. Kristensson, A. Ehn, A comprehensive study on dynamics of flames in a nanosecond pulsed discharge. Part II: plasma-assisted ammonia and methane combustion, Combust. Flame 275 (2025) 114076.

[14] S. Wang, X. Wei, M. Gu, Q. Lin, G. Luo, F. Hu, Flame characteristics and NO emission law of sliding arc plasma-assisted ammonia combustion, Combust. Flame 274 (2025) 114000.

[15] M. Li, Z. Wang, R. Xu, X. Zhang, Z. Chen, Q. Wang, Advances in plasma-assisted ignition and combustion for combustors of aerospace engines, Aero. Sci. Technol. 117 (2021) 106952.

[16] S. Birania, A.K. Attkan, S. Kumar, N. Kumar, V.K. Singh, Cold plasma in food processing and preservation: a review, J. Food Process. Eng. 45 (2022) e14110.

[17] S. Sumariyah, I. Hanafi, Z. Muchisin, F. Arianto, M. Nur, Comparison between corona and dielectric barrier discharge plasma using pin-to-single and dual ring electrode configurations, in: IOP Conference Series: Materials Science and Engineering, 434, 2018 012024.

[18] S. Bonuso, P. Di Gloria, G. Marseglia, R.A.O. Martínez, G. Mehdi, Z.A. Shah, A. Ficarella, M.G. De Giorgi, Investigation into the effect of H_2-enriched conditions on the structure and stability of flames in a low-swirl combustor derived from aero-engine design, Aerospace 11 (2024).

[19] H. Jakob, M.K. Kim, Generation of non-thermal plasmas over large and complex surfaces, Plasma Res. Express 2 (2020) 035010.

[20] J. Sun, W. Cui, Y. Tang, C. Kong, S. Li, Inlet pulsation-induced extinction and plasma-assisted stabilization of premixed swirl flames, Fuel 328 (2022) 125372.

[21] R. Feng, J. Li, Y. Wu, M. Jia, D. Jin, Ignition and blow-off process assisted by the rotating gliding arc plasma in a swirl combustor, Aero. Sci. Technol. 99 (2020) 105752.

[22] R.A. Varella, J.C. Sagás, C.A. Martins, Effects of plasma assisted combustion on pollutant emissions of a premixed flame of natural gas and air, Fuel 184 (2016) 269–276.

[23] Y. Tian, J. Zhu, M. Sun, H. Wang, Y. Huang, R. Feng, B. Yan, Y. Sun, Z. Cai, Enhancement of blowout limit in a Mach 2.92 cavity-based scramjet combustor by a gliding arc discharge, Proc. Combust. Inst. 39 (2023) 5697–5705.

[24] Y. Tian, J. Zhu, M. Sun, M. Wan, Y. Sun, B. Yan, T. Luo, Z. He, H. Wang, Combustion enhancement in a model scramjet by a simple pin-to-pin AC arc plasma, Proc. Combust. Inst. 40 (2024) 105259.

[25] G. Mehdi, D. Fontanarosa, S. Bonuso, M.G. De Giorgi, Ignition thresholds and flame propagation of methane–air mixture: detailed kinetic study coupled with electrical measurements of the nanosecond repetitively pulsed plasma discharges, J. Phys. Appl. Phys. 55 (2022) 315202.

[26] G. Mehdi, S. Bonuso, M.G. De Giorgi, Plasma assisted re-ignition of aeroengines under high altitude conditions, Aerospace 9 (2022) 66.

[27] G. Mehdi, S. Bonuso, M.G. De Giorgi, Development of plasma actuators for re-ignition of aeroengine under high altitude conditions, in: IOP Conference Series: Materials Science and Engineering, 1226, 2021 012034.

[28] M.G. De Giorgi, S. Bonuso, G. Mehdi, M. Shamma, S.R. Harth, N. Zarzalis, D. Trimis, Enhancement of blowout limits in lifted swirled flames in methane–air combustor by the use of sinusoidally driven plasma discharges, Notes on Numerical Fluid Mechanics and Multidisciplinary Design 152 (2022) 66–82.

[29] M.G. De Giorgi, G. Mehdi, S. Bonuso, M. Shamma, S. Harth, D. Trimis, N. Zarzalis, Characterization of flame behavior and blowout limits at different air preheating temperatures in plasma-assisted stabilized combustor, in: Proceedings of ASME Turbo Expo 2022: Turbomachinery Technical Conference and Exposition, Rotterdam, the Netherlands, 2022. Paper No. GT2022-83239.

[30] S. Bonuso, G. Mehdi, M.G. De Giorgi, Analysis of the premixed methane/air flames near lean blowout in plasma-assisted swirl combustor, in: Proceedings of the EUCASS 2022 Conference, 2022.

[31] A. Ercole, et al., Large eddy simulations of a turbulent premixed swirling flame with finite-rate chemistry and flame-wrinkling turbulent combustion models, Flow Turbul. Combust. (2025).
[32] C. Banyon, J.J. Rodriguez-Henriquez, G. Paterakis, Z. Malliotakis, K. Souflas, C. Keramiotis, G. Vourliotakis, F. Mauss, H.J. Curran, G. Skevis, P. Koutmos, M. Founti, A comparative study of the effect of varied reaction environments on a swirl-stabilized flame geometry via optical measurements, Fuel 216 (2018) 826–834.
[33] C. Ruan, F. Chen, W. Cai, Y. Qian, Y. Liang, X. Lu, Principles of non-intrusive diagnostic techniques and their applications for fundamental studies of combustion instabilities in gas turbine combustors: a brief review, Aero. Sci. Technol. 84 (2019) 585–603.
[34] D. Di, Y. Yan, Y. Liu, Study on the flow characteristics and oscillating mechanism of a swirl flame, Fuel 306 (2021) 121657.
[35] C. Ruan, F. Chen, T. Yu, W. Cai, X. Li, X. Lu, Experimental characterization of flame/flow dynamics during transition between stable and thermo-acoustically unstable conditions in a gas turbine model combustor, Aero. Sci. Technol. 102 (2020) 105858.
[36] J.L. Lumley, Computational modelling of turbulent flows, Adv. Appl. Mech. 18 (1979) 123–176.
[37] L. Sirovich, M. Kirby, M. Winter, An eigenfunction approach to large-scale transitional structures in jet flow, Phys. Fluids 2 (1990) 127–136.
[38] M.G. De Giorgi, D. Fontanarosa, A. Ficarella, E. Pescini, Effects on performance, combustion and pollutants of water emulsified fuel in an aeroengine combustor, Appl. Energy 260 (2020) 114263.
[39] C. Duwig, S. Ducruix, D. Veynante, Studying the stabilization dynamics of swirling partially premixed flames by proper orthogonal decomposition, J. Eng. Gas Turbines Power 134 (2012) 101501.
[40] O.T. Schmidt, T. Colonius, Guide to spectral proper orthogonal decomposition, AIAA J. 58 (2020) 1023–1033.
[41] L. Hu, Y. Luo, S. Han, Y. Wang, C. Wu, R. Ma, The source localization and dynamical evolution of axisymmetric screech modes in underexpanded supersonic jets, Aero. Sci. Technol. 140 (2023) 108427.
[42] F.J. Salvador, M. Carreres, J. García-Tíscar, M. Belmar-Gil, Modal decomposition of the unsteady non-reactive flow field in a swirl-stabilized combustor operated by a lean premixed injection system, Aero. Sci. Technol. 112 (2021) 106622.
[43] A. Cammilleri, F. Guéniat, J. Carlier, L. Pastur, E. Mémin, F. Lusseyran, G. Artana, POD-spectral decomposition for fluid flow analysis and model reduction, Theor. Comput. Fluid Dynam. 27 (2013) 787–815.
[44] M.G. De Giorgi, P. Di Gloria, D. Fontanarosa, A. Ficarella, Advanced multiscale modal and frequency analysis of swirling spray flame near lean blowout, Case Stud. Therm. Eng. 60 (2024) 104651.
[45] R.J. Moffat, Describing the uncertainties in experimental results, Exp. Therm. Fluid Sci. 1 (1988) 3–17.
[46] H.W. Coleman, W.G. Experimentation Steele, Validation, and Uncertainty Analysis for Engineers, third ed., John Wiley & Sons, Hoboken, 2009.
[47] A.M. Kypraiou, A.P. Dowling, E. Mastorakos, N. Karimi, Proper orthogonal decomposition analysis of a turbulent swirling self-excited premixed flame, in: Proceedings of the 53rd AIAA Aerospace Sciences Meeting, 2015. Paper No. AIAA 2015-0425.
[48] J.L. Lumley, The structure of inhomogeneous turbulence, in: Atmospheric Turbulence and Wave Propagation, 1967, pp. 166–178.
[49] A. Towne, O.T. Schmidt, T. Colonius, Spectral proper orthogonal decomposition and its relationship to dynamic mode decomposition and resolvent analysis, J. Fluid Mech. 847 (2018) 821–867.
[50] P.D. Welch, The use of fast Fourier transform for the estimation of power spectra: a method based on time averaging over short, modified periodograms, IEEE Trans. Audio Electroacoust. 15 (1967) 70–73.
[51] X. He, X. Fang, G. Rigas, M. Vahdati, Spectral proper orthogonal decomposition of compressor tip leakage flow, Phys. Fluids 33 (2021) 105105.
[52] Y.-F. Sang, D. Wang, J.-C. Wu, Entropy-based method of choosing the decomposition level in wavelet threshold de-noising, Entropy 12 (2010) 1499–1513.
[53] C.E. Shannon, A mathematical theory of communication, Bell Syst. Tech. J. 27 (1948) 379–423.
[54] E. Pescini, L. Francioso, M.G. De Giorgi, A. Ficarella, Investigation of a micro dielectric barrier discharge plasma actuator for regional aircraft active flow control, IEEE Trans. Plasma Sci. 43 (2015).
[55] G. Mehdi, S. Bonuso, M.G. De Giorgi, Identification of flow structures in a closed chamber in the presence of a needle plasma actuator, Phys. Fluids 34 (2022) 127118.
[56] T. Li, I.V. Adamovich, J.A. Sutton, Effects of non-equilibrium plasmas on low-pressure, premixed flames. Part 1: CH* chemiluminescence, temperature, and OH, Combust. Flame 165 (2016) 50–67.
[57] G. Mehdi, M.G. De Giorgi, S. Bonuso, Z.A. Shah, G. Cinieri, A. Ficarella, Comparative analysis of flame propagation and flammability limits of CH_4/H_2/air mixtures with or without nanosecond plasma discharges, Aerospace 10 (2023) 224.
[58] R. Rajasegar, C.M. Mitsingas, E.K. Mayhew, J. Yoo, T. Lee, Proper orthogonal decomposition for analysis of plasma-assisted premixed swirl-stabilized flame dynamics, IEEE Trans. Plasma Sci. 44 (2016) 2940–2951.
[59] R. Bompelly, T. Lieuwen, J. Seitzman, Lean blowout and its sensing in the presence of combustion dynamics in a premixed swirl combustor, in: Proceedings of the 47th AIAA Aerospace Sciences Meeting Including the New Horizons Forum and Aerospace Exposition, 2009. Paper No. AIAA 2009-982.
[60] G. Thampi, R.I. Sujith, Intermittent burst oscillations: signature prior to flame blowout in a turbulent swirl-stabilized combustor, J. Propul. Power 31 (2015) 1661–1671.
[61] R. Santhosh, S. Basu, Transitions and blowoff of unconfined non-premixed swirling flame, Combust. Flame 164 (2016) 35–52.
[62] S. Nair, T. Lieuwen, Acoustic detection of blowout in premixed flames, J. Propul. Power 21 (2005) 32–39.
[63] Z. Xi, Z. Fu, X. Hu, S.W. Sabir, Y. Jiang, An experimental investigation on flame pulsation for a swirl non-premixed combustion, Energies 11 (2018) 1757.
[64] Z. Cao, X. Yu, J. Peng, B. Hu, Z. Wang, Y. Yu, L. Gao, M. Han, X. Yuan, G. Wu, Flame features and oscillation characteristics in near-blowout swirl-stabilized flames using high-speed OH-PLIF and mode decomposition methods, Chin. J. Aeronaut. 36 (2023) 191–200.